Recent developments in frequency domain multi-axial fatigue analysis ♣

Denis Benasciutti [a*], Frank Sherratt [b], Alessandro Cristofori [a]

[a] University of Ferrara, Department of Engineering, via Saragat 1, 44122 Ferrara, Italy

[b] Engineering consultant, Rugby, CV23 0LG, United Kingdom

Abstract

The purpose of this paper is to discuss the recent developments in multi-axial spectral methods, used for estimating fatigue damage of multi-axial random loadings from Power Spectral Density (PSD) data. The difference between time domain and frequency domain approaches in multi-axial fatigue is first addressed, the main advantages of frequency domain approach being pointed out. The paper then critically reviews some categories of multi-axial spectral methods: approaches based on uniaxial equivalent stress (strength criteria, "equivalent von Mises stress", multi-axial rainflow counting), critical plane criteria (Matake, Carpinteri-Spagnoli, criterion based on resolved shear stress on critical plane), stress-invariants based criteria (Crossland, Sines, "Projection-by-Projection"). The "maximum variance" method and the Minimum Circumscribed Circle/Ellipse formulations defined in the frequency domain are also discussed. The paper critically analyses also non-proportional multi-axial loadings and the role of material fatigue parameters (e.g. S/N curves for bending/torsion) in relation to specific methods. The paper concludes with general comments on advantages and possible limitations in the use of multi-axial spectral methods, with special focus on the assumption of stationarity and Gaussianity in modelling multi-axial random loadings.

Keywords

multi-axial random stress, fatigue, Power Spectral Density (PSD), spectral methods

♣ This paper is dedicated to the memory of prof. Frank Sherratt, who inspired this research and offered wise advices when writing the manuscript. It is a great sadness that he would not see this work published.

* Corresponding author. E-mail: denis.benasciutti@unife.it
Phone: +39 (0)532 974976, Fax. +39 (0)532 974870

1 Introduction

The estimation of fatigue life under multi-axial loading has been an active research topic in the last fifty years and the activity has further increased in the last decades [1]. One reason may be the increased use of Finite Element (FE) analysis in the design of mechanical components. Nowadays, any FE software is capable to afford the analysis of complex component geometries under any type of loading (e.g. variable amplitude or random). The software outputs are the time histories of the full stress tensor (multi-axial stress) at each node in the model [2].

In the literature, a large number of theories and criteria have been proposed to estimate fatigue life under multi-axial loading [3-5]. Such theories can be classified as "time domain" approaches, as they apply deterministic algorithms directly to digitalised samples of stress time histories obtained from FE analysis [6-10]. Such deterministic algorithms can be used, for example, to locate the critical plane or to measure the amplitude of the second invariant of the stress deviator [5,9]. Despite continuous improvements [11-15], the computation time of the existing algorithms remains high and it increases exponentially with the number of sample points being processed. The computation time can even become excessive when processing random time-histories of thousands of points, which are simulated in finely discretised three-dimensional FE models with a huge number (e.g. hundreds of thousands) of nodes [8,16,17]. This could be a severe limitation in situations (for example, in industrial practice) where multi-axial FE analysis has to be completed in the shortest time possible.

The "frequency domain" (or spectral) approach seems to offer this advantage and it has been suggested as a possible alternative to time domain one for the analysis of multi-axial random stresses [18]. In frequency domain approach, multi-axial random stresses are conveniently characterised in the frequency domain by a set of Power Spectral Density (PSD) functions [19,20].

Methods for estimating the fatigue life from PSD functions have been developed, compared with time domain results and then confirmed by laboratory experiments mainly for uniaxial random loadings. Although deriving spectral methods for multi-axial random loading may appear as an obvious step forward from uniaxial solutions, it is instead a challenging task that has been the major activity for several research groups over the last decades. Despite the complexity of the spectral approach in multi-axial fatigue, however, some underlying principles are beginning to emerge, which this paper tries to codify by a critical analysis of several theories from the literature. Experience in the development of spectral methods for uniaxial random loadings is also considered in the comparison with the multi-axial case.

This paper is not intended to be neither a simple review of the existing literature, nor merely a comparison of spectral methods. Instead, its main purpose is to exploit a literature survey to recognise general principles in spectral fatigue analysis and, hopefully, to identify those methods that are theoretically well founded and more accurate.

2 Motivation for spectral analysis in multi-axial fatigue

While multi-axial fatigue criteria developed as in time domain approaches are generally well known, multi-axial spectral methods in frequency domain has often been viewed with suspicion. Engineers are often tempted to question whether frequency domain approach can really provide some advantages compared to time domain analysis. A possible answer can be given by looking at the type of loading (deterministic or random) and the computation time in multi-axial fatigue analysis.

A first important distinction is between deterministic and random loadings. In deterministic loads (e.g. constant amplitude loadings), future values can be calculated exactly from present or past values. In random loadings (e.g. the road excitation in a car, the action of wind or waves on structures), future values cannot be exactly predicted from present or past values, but only estimated by probabilistic methods [21]. A statistical approach is then needed to correctly analyse the outcomes of multi-axial criteria applied to random loadings.

For example, if life estimation has to be carried out on a component, subjected to service loads that are stationary random over significant periods, statistical methods will have to be used. A large FE model will be normal and even with the best algorithms the computational load will be substantial. Using FE encourages the use of multi-axial theories, which further increases this computational load. Most commercial FE suites include frequency domain analysis, but this is normally used only to estimate the response of the loaded component.

Fatigue life estimation under uniaxial load from frequency domain data is now an accepted practice in some branches of engineering though, and there are reports of some successful applications to the multi-axial case [22,23]. If stationary random records of service loading are available, a designer may be able to choose to work in the time domain or in the frequency domain. Computational efficiency will then be the main criterion for selecting the most useful approach.

In time domain approach, step-by-step algorithms are directly applied to random multi-axial stress time-histories (obtained by measurements or FE simulations). Results depend on the particular set of time-histories being analysed, which are not exactly identical from one record to the other.

Therefore, time domain results from replicated time-history records show a statistical variability, as it will be shown by the example discussed in Section 3.2.

Replicated records or very long time-histories are thus needed to assure that results are statistically stable [20,24]. Simulating long time-histories in large or even medium size FE models usually increases the computation time, especially when non-linearity or contact elements are included [20]. Also the processing time for multi-axial fatigue analysis may become prohibitive, when analysing time-histories in each node of FE model (in critical plane approach, for example, a huge number of planes have to be scanned in the whole FE model) [20]. In FE multi-axial fatigue analysis, the time-history length is then a trade-off between statistical scatter and processing time.

The above issues can be overcome by using a frequency domain (spectral) approach to multi-axial fatigue, where multi-axial random time-histories are characterised by a Power Spectral Density (PSD) matrix $\mathbf{S}(\omega)$, which is formally defined as the Fourier transform of the autocorrelation matrix $\mathbf{R}(\delta)$ (Wiener-Khinchine theorem) [19, 25]:

$$\mathbf{S}(\omega) = \int_{-\infty}^{\infty} \mathbf{R}(\delta)\, e^{-i\omega\delta}\, \mathrm{d}\delta \tag{1}$$

where δ is a time lag and i is the imaginary unit. PSD functions are normally estimated directly from digitalized time-history records by well-known techniques (e.g. Welch's method) [25].

Spectral fatigue analysis in frequency domain has several advantages compared to time domain analysis. For example, the scatter in the estimated PSD tends to be less relevant, because only average quantities (e.g. spectral moments λ_n and bandwidth parameters) are used in multi-axial spectral methods. For instance, [26] studied the uncertainty in spectral parameters which results from the particular technique used to estimate the PSD (e.g. Blackman–Tukey, FFT with various segment averaging, maximum entropy). The study considered spectral parameters used in ocean engineering, which are, however, very similar to the parameters used in spectral fatigue. The results showed how spectral parameters that depend on the overall PSD are not influenced by the particular spectral estimation procedure; instead, tapering the time-history before PSD estimation has some influence [26].

One advantage of the frequency domain approach is that it can apply the random process theory to derive important properties of random signals. For a stationary Gaussian uniaxial stress, for example, several quantities used in fatigue analysis (e.g. peaks/valleys distribution, frequency of peaks and upward crossings, irregularity factor) can be calculated from the stress PSD by simple

analytical expressions [27-29]. In uniaxial random signals, spectral methods also allow analytical expression to be used for estimating the rainflow cycle distribution and fatigue damage directly from PSD data [27-29]. With multi-axial random loadings, this theoretical framework can be extended to allow time domain multi-axial criteria to be re-formulated in the frequency domain [19]. This makes the spectral approach very powerful especially with FE simulations, where it can be combined with frequency domain dynamic analysis to obtain a quick fatigue life assessment of the component, which is particularly convenient at the early design stage [20].

3 Survey on selected multi-axial spectral methods

Multi-axial spectral methods are generally obtained as frequency domain re-formulations of time domain criteria. Adopting the same classification scheme used for time domain criteria, among all existing criteria we can distinguish: criteria based on equivalent uniaxial stress, critical plane criteria, methods based on stress-invariants. This Section provides a survey on some selected multi-axial spectral methods following this classification. General remarks on some special features are discussed in Section 4.

3.1 Criteria based on equivalent uniaxial stress

This class of criteria transforms a multi-axial stress into a uniaxial equivalent stress, which is assumed to cause the same amount of fatigue damage as the multi-axial stress. The use of a uniaxial equivalent stress is particularly convenient, as it opens up the possibility to use spectral methods for uniaxial random loadings to estimate the fatigue damage of multi-axial loadings. Some well-known methods are the “narrow-band formula”, Dirlik expression, TB method, “single-moment” method, just to cite a few examples [27-32]).

The accuracy of the estimation depends, of course, on the particular definition of equivalent stress and on the accuracy of the uniaxial spectral method that is adopted. Among the multitude of uniaxial spectral methods now available in the literature, some methods (Dirlik, TB method) have shown a far superior accuracy (especially with wide-band random loading), as confirmed by numerical comparisons carried out by several independent studies [33-35].

Please insert here Figure 1

The significant point, though, is not which uniaxial formula gives good life predictions but whether or not a particular proposal for "equivalence" allows those expressions to make good estimates. Niesłony et al. [36] report tests showing successful use of Dirlik and TB formulae following application of one particular equivalence criterion. Figure 1 shows the results.

Note that also the C-S criterion described in Section 3.2.2 can be classified, to some extent, as a criterion based on equivalent stress, as it computes an equivalent PSD based on the PSDs of normal and shear stress acting on the critical plane, see Eq. (11).

3.1.1 Generalisation of strength criteria to random loadings

Macha and co-workers were perhaps the first to re-formulate static strength criteria in the frequency domain to define multi-axial spectral methods for random loadings; Refs. [19,37] provides a survey on such criteria. Among them, some noteworthy examples are: criterion of the maximum normal stress, normal strain or shear stress in the fracture plane, criterion of the maximum principal stress (Galileo's hypothesis), Tresca and von Mises stress.

Such criteria define an equivalent uniaxial stress $\sigma_{eq}(t)$ that is a combination of the components $\sigma_i(t)$ of the stress vector. The relationship between $\sigma_{eq}(t)$ and $\sigma_i(t)$ is established by the expression of the static strength theory, or it is a function of some direction cosines that locate a physical plane (e.g. the fracture plane).

Depending on the type of criterion, the relationship between $\sigma_{eq}(t)$ and $\sigma_i(t)$ can be linear or non-linear. For linear criteria (e.g. maximum normal stress, normal strain and shear stress on the fracture plane) the equivalent uniaxial stress is defined as:

$$\sigma_{eq}(t) = \sum_{i=1}^{6} a_i \, \sigma_i(t) \qquad\qquad S_{eq}(\omega) = \sum_{h=1}^{6}\sum_{k=1}^{6} a_h a_k S_{hk}(\omega) \tag{2}$$

where a_i are direction cosines. The linear relationship in Eq. (2) allows also the PSD of the equivalent stress $S_{eq}(\omega)$ to be calculated by linear combination of stress PSDs.

Instead, some other criteria (e.g. criterion of the maximum principal stress, von Mises stress) are expressed by non-linear equations, which cause the frequency spectrum to be distorted (e.g. the equivalent stress has a wider frequency band than the stress components). Furthermore, a non-linear equation transforms Gaussian stress components into a non-Gaussian equivalent stress. The limitations of using a non-linear expression for von Mises stress criterion in the frequency domain have been solved by the approach proposed by Preumont et al., discussed in the next Section.

The definition of an equivalent uniaxial stress makes also possible to apply the "variance method" [38,39,40] to identify the fracture plane, as the plane where the equivalent stress reaches its maximum variance (the variance method is also adopted by the criterion described in Section 3.1.4).

3.1.2 "Equivalent von Mises stress"

This is perhaps the most popular multi-axial spectral method based on equivalent stress. The frequency domain formulation comes from the definition of von Mises stress, which for a biaxial state of stress is:

$$\sigma_{vm}^2(t) = \sigma_{xx}^2(t) + \sigma_{yy}^2(t) - \sigma_{xx}(t)\sigma_{yy}(t) + 3\tau_{xy}^2(t) \tag{3}$$

Owing to the quadratic form of Eq. (3), the von Mises stress is a random process that is always positive, non-Gaussian, nor zero-mean, even if all stress components are zero-mean and Gaussian [37]. Furthermore, the frequency content of $\sigma_{vm}(t)$ is not consistent with that of stress components. In fact, in Eq. (3) the squared terms give frequency peaks at twice the frequencies (doubling) of the original PSDs, while the cross-product $\sigma_{xx}(t)\cdot\sigma_{yy}(t)$ gives additional contributions by a frequency shift of the original PSDs of $\sigma_{xx}(t)$ and $\sigma_{yy}(t)$. Therefore, the PSD of the von Mises stress cannot be obtained by a simple linear combination of PSDs of the components of stress.

To overcome these inconsistencies, Preumont et al. introduced an "equivalent von Mises stress" (EVMS) $\sigma_{eq}(t)$, which is a uniaxial Gaussian random stress with the following PSD (**Q** is a matrix of constants) [41,42]:

$$S_{vm}(\omega) = \text{trace}\left\{\mathbf{Q}\,\mathbf{S}(\omega)\right\} = S_{xx}(\omega) + S_{xx}(\omega) - \text{Re}\left\{S_{xx,\,yy}(\omega)\right\} + 3S_{xy}(\omega) \tag{4}$$

The EVMS $\sigma_{eq}(t)$ must not be confused with the von Mises stress in Eq. (3), as the EVMS follows from the PSD defined in (4) and thus it has all the properties we were looking for: it is zero-mean and Gaussian, with variance equal to the sum of the variances of the stress components.

The basic assumption of the EVMS criterion is that the equivalent stress $\sigma_{eq}(t)$ causes the same fatigue damage as the multi-axial stress $\sigma_{xx}(t)$, $\sigma_{yy}(t)$, $\tau_{xy}(t)$. The fatigue damage of $\sigma_{eq}(t)$ can be estimated by the spectral methods for uniaxial stress.

Thanks to its simplicity and its ease of use, the EVMS method has found wide use in academic and applied research [42-47]. In addition, the theoretical framework of EVMS criterion was also used to

reformulate in the frequency domain other multiaxial fatigue criteria (e.g. multiaxial rainflow counting, Crossland and Sines criteria), which will be discussed in Sections 3.1.3 and 3.3.

Although not explicitly mentioned, the EVMS is based on to inherent hypotheses: i) the S-N fatigue lines for normal and shear stress have equal inverse slopes $k_\sigma=k_\tau$, ii) the fatigue limits $\sigma_{\infty-1}$, $\tau_{\infty-1}$ (or, equivalently, the fatigue strengths σ_A, τ_A at $N_A=2\cdot10^6$ cycles) under fully-reversed bending and torsion are exactly scaled by $\sqrt{3}$. When such hypotheses are not satisfied, the EVMS criterion can lead to large errors in damage estimation, as it will be extensively discussed in Section 4.1.

These potential drawbacks of Preumont's EVMS criterion were firstly pointed out in [48] and then in [49] (which also proposed a modified version of EVMS in deviatoric space). Other modifications of the original Preumont's EVMS suggested by Braccesi [50] and Niesłony [51,52] provide improved estimations [53]. The version of Niesłony has been shown to provide good estimates compared to experimental results for bending-torsion random loading, see Figure 1.

3.1.3 Multi-axial rainflow counting

The rain-flow method is now recognised as the best counting method in uniaxial variable amplitude and random loadings. Over the last decades, several attempts have been proposed to codify a multi-axial rainflow counting, which extends the rain-flow method also to multi-axial loadings [54-59].

Among them, the method proposed in [54,56] suggests to count the rain-flow cycles and to compute the fatigue damage on an equivalent uniaxial stress, which is defined as a linear combination of stress components. For a biaxial stress $\sigma_{xx}(t)$, $\sigma_{yy}(t)$, $\tau_{xy}(t)$, the equivalent stress is:

$$\sigma_m(t) = c_1\sigma_{xx}(t) + c_2\sigma_{yy}(t) + c_3\tau_{xy}(t) \tag{5}$$

where the constants satisfy $c_1^2 + c_2^2 + c_3^2 = 1$. The method scans all possible linear combinations and seeks the one that leads to the largest value of calculated fatigue damage.

Thanks to linearity, the method based on expression (5) has been re-formulated in the frequency domain in [42]. In particular, the same theoretical framework of the EVMS criterion is used to compute the PSD of the equivalent stress $\sigma_m(t)$ as:

$$S_m(\omega) = \text{trace}\left\{\mathbf{Q}^* \mathbf{S}(\omega)\right\} \tag{6}$$

where $\mathbf{Q^*}$ is a matrix that contains the constants c_1, c_2, c_3. The PSD in (6) allows the damage of the equivalent stress to be estimated by the spectral methods for uniaxial loadings. This frequency

domain formulation then allows a quick scan of all possible linear combinations, to identify the most critical one.

3.1.4 Resolved shear stress on critical plane

This is a critical plane criterion that can also be classified in equivalent-stress based criteria, as it looks at the shear stress resolved along a specified direction on the critical plane [60].

This criterion is formulated by considering a Cartesian reference frame Oxyz with origin O, which is a point in a body where crack initiation may occur, see Figure 2. The axes *x*, *y* define a plane Π with normal *z*. Now consider a material plane Δ with normal **n**, and define a local reference frame Oabn, where **a** and **b** are unit vectors. Figure 2 shows that the plane Δ is uniquely defined by the two angles θ and φ. The interest is now on a generic direction **m** on plane Δ, which is identified by the angle α between vectors **a** and **m**.

Please insert here Figure 2

This multi-axial spectral method looks at the shear stress $\tau_m(t)$ on plane Δ and resolved along **m**. For a biaxial state of stress, the stress $\tau_m(t)$ is calculated by the scalar product [60,61]:

$$\tau_m(t) = \mathbf{q} \bullet \mathbf{x}(t) \qquad \mathbf{q} = \begin{bmatrix} \frac{1}{2}\left(\sin(\theta)\sin(2\varphi)\cos(\alpha) + \sin(\alpha)\sin(2\theta)\cos(\varphi)^2 \right) \\ \frac{1}{2}\left(\sin(\theta)\sin(2\varphi)\cos(\alpha) + \sin(\alpha)\sin(2\theta)\sin(\varphi)^2 \right) \\ \frac{1}{2}\sin(\alpha)\sin(2\varphi)\sin(2\theta) - \cos(\alpha)\cos(2\varphi)\sin(\theta) \end{bmatrix} \tag{7}$$

where **q** is a constant vector of direction cosines (which only depends on the angles that locate the plane Δ) and $\mathbf{x}(t)=(\sigma_{xx}(t), \sigma_{yy}(t), \tau_{xy}(t))$ is the stress vector (note that previous expression (7) can also be extended to a three-dimensional state of stress [62]).

For random loading, the resolved shear stress $\tau_m(t)$ is a uniaxial random process. Therefore, the critical plane Δ^* can be identified in a statistical sense, by looking at the plane where stress $\tau_m(t)$ reaches its maximum variance. The variance of $\tau_m(t)$ can be calculated as:

$$\mathrm{Var}\left(\tau_m(t)\right) = \mathbf{q}^T \mathbf{C}\, \mathbf{q} \tag{8}$$

where **C** is the covariance matrix of the stress. The position of the direction **m** on the plane Δ only depends on the angles θ, φ, α, which define vector **q**. Then, the variance $Var(\tau_m(t))$ in (8) depends on angles θ, φ, α as well. The direction of maximum variance of stress $\tau_m(t)$ can be found by solving a problem of maximum for $Var(\tau_m(t))$, according to the "variance method" [38,39,40].

When the critical plane, located by angles (θ^*, φ^*, α^*), has been identified, the multi-axial stress is transformed to the uniaxial stress $\tau_m(t)$), which is then assumed to cause the same fatigue damage as the multi-axial stress. This transformation allows the use of uniaxial spectral methods to estimate the fatigue damage of $\tau_m(t)$ for a multi-axial stress.

Ref. [60] applied this multi-axial spectral method to the fatigue durability assessment of a vehicle in a virtual bench test (four post test rig), simulating a driving test over a road pavé. In the bench test, the vehicle is subjected to vertical displacement histories, which reproduce the experimental accelerations of a 60-sec driving test at an average speed of 35 km/h. The vehicle dynamic response and the stress histories were calculated by a Multi-Body/Finite Element analysis in time domain.

The peculiarity of this example is that the input displacements applied to the vehicle slightly deviated from the Gaussian probability distribution (i.e. they were non-Gaussian). As a result, also the local multi-axial stress and the resolved shear stress $\tau_m(t)$ were non-Gaussian. This situation was solved by applying the TB method for non-Gaussian random loadings [63,64]. The simulations in Ref. [60] confirmed a quite good agreement between frequency domain and time domain results.

3.2 Critical plane criteria

This class of multi-axial criteria looks at the physical plane where crack nucleation and propagation is likely to occur. This plane usually experiences the highest shearing stress in crack initiation and the highest normal stress in crack propagation. Most multi-axial damage expressions in critical plane criteria then contain a shearing stress τ, a normal stress σ, or their combination. The ratio σ/τ will depend on the instantaneous values of the loads on the two (or three) axes, in addition to the variation due to planar orientation.

In random loading, the normal component σ is a uniaxial scalar random stress, which can be characterised in the frequency domain with no particular effort. The shearing stress, instead, is a vector process $\boldsymbol{\tau}(t)$ and calculating its amplitude τ_a in frequency domain is a more challenging task. The tip of $\boldsymbol{\tau}(t)$ describes a curve Ψ called "loading path", which is closed for periodic loading, not closed for non-periodic ones, whereas it is an irregular coiled curve for random loading, see Figure 3.

Please insert here Figure 3

Defining the maximum amplitude τ_a of the loading path Ψ is a non-trivial problem, which is solved by adopting conventional definitions [9]. For example, in the Minimum Circumscribed Circle (MCC) method the shear amplitude τ_a is measured by the radius of the minimum circle circumscribing the loading path [9]. The same circle, however, can enclose loading paths having quite different shapes (e.g. same length but different widths), which are then not correctly discriminated. An alternative definition that can distinguish such situations, measuring both the length and width of loading path, is the Minimum Circumscribed Ellipse (MCE), which defines the amplitude τ_a by a quadratic sum of the semi-axes of the enclosing ellipse [65], see Figure 3(a).

Please insert here Figure 4

The MCC/MCE definitions are usually implemented in step-by-step algorithms, which are applied directly to a sample path Ψ to calculate the amplitude τ_a [12,13]. Of course, the calculated value of τ_a strictly depends on the circle/ellipse circumscribing the particular path Ψ that has been processed; the amplitude τ_a is then a univocal property of Ψ.

In deterministic loading, the sample path Ψ is uniquely defined (deterministic); then, only one circle/ellipse is found and the amplitude τ_a takes a unique value. In random loading, instead, the sample path Ψ is scattered, as shown in the examples of Figure 4. This means that small differences are always observed even among sample curves Ψ that are obtained from replicated simulations or measurements under virtually identical conditions. Such differences in replicated samples of Ψ then lead to differences in the calculated MCC/MCE and then to a scatter in the obtained values of τ_a, which is then a random variable.

The scatter in time domain results is confirmed by the results in Figure 4 and Table 1. Figure 4 compares three replicated simulations of random paths Ψ of two multi-axial loadings with different correlation (r=0.0, r=0.99). The variance of each shear stress component is $Var(\tau_1(t))=Var(\tau_2(t))=1$. The load path has 2^{18} points. Although the statistical properties remain unchanged, the time domain results are similar but not exactly identical, see Table 1.

Please insert here Table 1

A frequency domain re-formulation of MCC/MCE definitions has been proposed for random loading, to provide a statistical measure of the amplitude τ_a. For example, an expected radius $E[R]$ based on the "maximum variance" concept is an intuitive measure of the expected amplitude $E[\tau_a]=E[R]$ on the critical plane, see Figure 3(b). The critical plane is then defined as the plane with the maximum expected radius $E[\tau_a]=E[\mathrm{R}]$. This leads to the definition of the Expected Minimum Circumscribed Circle (EMCC) [66].

The expected radius $E[\mathrm{R}]$ is estimated by Davenport's formula, which gives the largest maximum (in time interval T) of the projection $s_i(t)$ of loading path along the direction of maximum variance:

$$E(R_i) = E\left(\underset{0\le t\le T}{Max}\left(s_i(t)\right)\right) = \sigma_i\left(\sqrt{2\ln(\nu_{0,i}^{+}\,T)} + \frac{0.5772}{\sqrt{2\ln(\nu_{0,i}^{+}\,T)}}\right) \tag{9}$$

where $\nu_{0,i}^{+} = \sqrt{\lambda_{2,i}/\lambda_{0,i}}$ is the frequency of mean up-ward crossings of the mean value $E[s_i(t)]$, which is estimated from the spectral moments $\lambda_{0,i}$, $\lambda_{2,i}$ of $s_i(t)$.

The result in expression (9) has been used in Refs. [67,68] to extend also the MCE definition to the frequency domain. In the Expected Minimum Circumscribed Ellipse (EMCE) definition, two semi-axes $E[R_1]$ and $E[R_2]$ are combined to define the expected shear stress amplitude as $E[\tau_a] = \sqrt{E[R_1]^2 + E[R_2]^2}$, to include the effect of non-proportional loading paths. The minor semi-axis $E[R_2]$ is taken along the direction of minimum variance of Ψ, see Figure 3(b).

The expression (9) is based on the hypothesis that adjacent maxima are independent and it tends to overestimate the extreme value for a narrow-band process [69,70]. Corrections of Davenport's formula (9) can also be used to account for bandwidth effects [69,70], without however altering the basic definition of EMCM/EMCE approach.

In some cases, MCC/MCE algorithms in time domain are so much influenced by the local shape of the loading path Ψ, that the calculated circle/ellipse curves are very close together, if not even coincident. This would give an incorrect measure of the real shape of Ψ (i.e. wrong measure of the degree of non-proportionality). Time domain results are also scattered, as already observed. The EMCC/EMCE definitions in frequency domain, instead, have the advantage to depend only on the statistical properties of the multi-axial random loading, summarised by its spectral parameters. This

clearly makes such spectral definitions definitively more stable and not affected by the statistical scatter observed in time domain results, see Figure 4.

The frequency domain definition of EMCC is used to define the critical plane orientation in the frequency domain formulation of Matake spectral method [66], described in Section 3.2.1. The spectral definition of EMCE has been used, instead, in the frequency domain formulation of Sines criterion [71], discussed in Section 3.3.2.

3.2.1 Matake criterion

This infinite life criterion is expressed as a linear combination of the amplitude of shear stress and the maximum of normal stress acting on the critical plane. The critical plane, located by two Euler angles (γ^*,φ^*), is defined as the plane where the amplitude of shear stress τ_a^* reaches its maximum value. In random loading, the amplitude τ_a^* is a random variable and the critical plane is identified by using the EMCC definition discussed in Section 3.2.

The definition of Matake criterion for random loading requires a probabilistic approach, which is a very complicated problem with no exact analytical solution, and which can be approached only by Monte Carlo simulations [66]. As a solution, Preumont et al. [66] proposed the following approximation:

$$\frac{E\left[\tau_a^*\right]+\alpha\left(\sigma_m^*+E\left[\sigma_a^*\right]\right)}{\rho}\leq 1 \tag{10}$$

which considers the expected values of the amplitude of shear stress, $E\left[\tau_a^*\right]$, and normal stress $E\left[\sigma_a^*\right]$ on the critical plane; σ_m^* is the mean value of the normal stress, which is zero for a zero-mean multi-axial random loading.

In expression (10), $\alpha=(2\tau_{\infty-1}/\sigma_{\infty-1})-1$, $\rho=\tau_{\infty-1}$ are material parameters derived from fatigue limits $\sigma_{\infty-1}$, $\tau_{\infty-1}$ in fully-reversed bending and torsion. Even if the existence of a fatigue limit has been called into question [72-75], we assume that a fatigue limit exists, since a debate on this topic would be outside the scope of this discussion. In the expression (10), the material fatigue properties (e.g. fatigue limits $\sigma_{\infty-1}$, $\tau_{\infty-1}$, or equivalently the fatigue strengths σ_A, τ_A at N_A cycles) are treated as deterministic quantities. For example, the fatigue strength could be referred to a given survival probability (e.g. P_s=90% or 97.7%) and estimated by statistical analysis of experimental data.

Instead, the expected values in (10) are further specialised by a frequency domain approach [66]. In particular, Davenport's formula, as that in expression (9), is used to estimate the expected amplitudes of shear $E\left[\tau_a^*\right]$ and normal stress $E\left[\sigma_a^*\right]$.

The numerical results in [66] for a L-shaped beam under random accelerations showed that Matake frequency domain formulation "*produces slightly conservative values when compared to those obtained with time domain simulations*" [66]. In particular, [66] reports a general close agreement for the calculated maximum shear stress in frequency domain, which was only 7 MPa in higher average compared to time domain results (with a maximum difference of 15 MPa). On the other hand, in the analysis of L-shaped beam the frequency domain formulation was able to reduce of three orders of magnitude the computation time (which strongly depends on the number of scanned planes).

3.2.2 Carpinteri-Spagnoli (C-S) method

In the original time domain version of this criterion [76,77], the critical plane is linked to the average principal stress directions $\hat{\mathbf{1}}$, $\hat{\mathbf{2}}$, $\hat{\mathbf{3}}$. In the case of multi-axial random loading, the average principal directions are identified by a statistical approach, formulated in the frequency domain.

The concept of "maximum variance" is used in the frequency domain C-S criterion to locate the critical plane [78].

The principal frame $\hat{\mathbf{1}}$, $\hat{\mathbf{2}}$, $\hat{\mathbf{3}}$ is the starting point to find the critical plane. The normal *w* to the critical plane is located by a rotation δ about the axis $\hat{\mathbf{2}}$, where δ is an off-angle that is a function of the ratio of fatigue limits $\sigma_{\infty-1}$, $\tau_{\infty-1}$ for fully-reversed normal and shear stress. A further rotation γ around the *w*-axis is finally necessary to find the directions *u*, *v* on the critical plane, which experiences the maximum and minimum variance of the stress, respectively [76-78].

Once the reference frame (*u*, *v*, *w*) on the critical plane has been identified (with a sequence of five rotations), the PSDs $S_{w,w}(\omega)$, $S_{vw,vw}(\omega)$ of the normal and shear stress, σ_w and τ_{vw}, are considered by simple matrix algebra. By this approach, the multi-axial stress has been transformed to a biaxial state of stress on the critical plane. As a final step, the biaxial stress on critical plane is condensed into a uniaxial equivalent normal stress $\sigma_{eq}(t)$, with PSD:

$$S_{eq}(\omega) = S_{w,w}(\omega) + \left(\frac{\sigma_{\infty-1}}{\tau_{\infty-1}}\right) S_{vw,vw}(\omega) \tag{11}$$

Having defined the PSD $S_{eq}(\omega)$, spectral methods for uniaxial loadings can be used to estimate the fatigue damage directly from $S_{eq}(\omega)$.

It is interesting to note that the equivalence rule in Eq. (11) correlates the frequency content of the uniaxial stress to the fatigue limits $\sigma_{\infty-1}$, $\tau_{\infty-1}$ for both normal and shear stress; this allows any combination of fatigue limits to be taken into account. On the other hand, the possible influence of the inverse slopes of S/N curve on the definition of the equivalent PSD $S_{eq}(\omega)$ (as it will be discussed in Section 4.1) is a matter that could be worth investigating.

Compared to its time domain original formulation, the frequency domain C-S spectral method provides a great simplification when searching the critical plane, thus reducing the computation time and increasing efficiency. Secondly, the definition of an equivalent stress on the critical plane, of course, allows using spectral methods for uniaxial stress (in [78] the TB method was used, but nothing prevent to adopt any other uniaxial spectral method).

3.3 Criteria based on stress invariants

3.3.1 Crossland criterion

Among stress-invariant based criteria, Crossland criterion was probably the first that has been re-formulated in frequency domain. This infinite-life criterion is expressed as a linear combination of the maximum amplitude of the second invariant of the stress deviator, $\sqrt{J_{2,a}}$, and the maximum value of the hydrostatic stress, $max[\sigma_H(t)]$. In random loading, $\sqrt{J_{2,a}}$ and $max[\sigma_H(t)]$ are random variables and the criterion has to be re-formulated by a probabilistic approach that relies on probability density functions of both variables. As for Matake criterion, the probabilistic definition of Crossland criterion is a very complicated problem that cannot be solved analytically. Preumont et al. then proposed a simple approximation using expected values:

$$\frac{E\left[\sqrt{J_{2,a}}\right]+\kappa\left(E\left[\max(\sigma_H(t))\right]\right)}{\rho}\leq 1 \tag{12}$$

Two different versions of expression (12) exist in the frequency domain [42,66]. In the first proposal [42], the expected value $E\left[\sqrt{J_{2,a}}\right]$ was approximated by the expected largest maximum of the "equivalent von Mises stress" (EVMS), already discussed in Section 3.1.2. The largest maximum is determined by Davenport's formula (9), or its corrections [69,70]. The same formula is

also used to estimate the expected maximum value of hydrostatic stress $\sigma_H(t)$. This approach leads to the following expression [42]:

$$\frac{\left(1/\sqrt{3}\right)\eta_{\text{EVMS}}\sqrt{Var(\sigma_{\text{eq}}(t))}+\kappa\,\eta_{\text{H}}\sqrt{Var(\sigma_{\text{H}}(t))}}{\rho} \tag{13}$$

where η_{EVMS} , η_{H} are, respectively, the peak factors for the EVMS and hydrostatic stress, which are given by Davenport's formula [69,70] (the peak factor is defined as the extreme value of the process normalised to the standard deviation; simple formulae for the peak factor are given in [70]). In expression (13), $\kappa=(3\tau_{\infty-1}/\sigma_{\infty-1})-\sqrt{3}$ and $\rho=\tau_{\infty-1}$ are material parameters, defined from the fatigue limits $\sigma_{\infty\text{-}1}$, $\tau_{\infty\text{-}1}$ in fully-reversed bending and torsion.

Although the frequency domain expression (13) showed a quite good agreement with time domain results [42], a modified version next proposed in [66] was presumed to give estimations more accurate than expression (13). This new formulation keeps the same approximation of the maximum hydrostatic stress; it proposes, instead, a different approximation for $E\left[\sqrt{J_{2,\text{a}}}\right]$, based on the expected amplitude of a loading path, by the formalism of the EMCC definition discussed in Section 3.2. The expected amplitude is equal to the expected radius of the smallest hyper-sphere circumscribed to the random loading path, described by the tip of a four-dimensional Gaussian vector process [66].

Numerical results for an L-shaped beam subjected to random accelerations showed that time domain calculations were in very close agreement with frequency domain estimations, obtained with both versions of Crossland criterion reviewed in this Section.

3.3.2 Sines criterion

As it is well known, Sines criterion is identical to Crossland one, except that it considers the mean value of hydrostatic stress, not the maximum value. This close similarity would allow the theoretical framework of Crossland criterion (discussed in Section 3.3.1) to be adapted also to re-formulate Sines criterion in the frequency domain, with very minor changes (the expected maximum of hydrostatic stress $E[\max(\sigma_H(t))]$ should only be replaced by the mean value $E[\sigma_H(t)]$).

The frequency domain formulation of Sines criterion here discussed is based, instead, on a different and quite interesting approach, developed by Lambert et al. [71]. The approach develops a

reliability model which estimates the probability density function of the random variable $\sqrt{J_{2,a}}$, and which also includes the uncertainty of material fatigue properties.

In random loading, the amplitude of the second invariant $\sqrt{J_{2,a}}$ is a random variable, as in Crossland criterion. The probability distribution of $\sqrt{J_{2,a}}$ is, however, not known. Results of numerical simulations allow [71] to suggest a Gumbel distribution:

$$p_{\sqrt{J_{2,a}}}(x) = \frac{1}{\beta}\exp\left(-\frac{x-\mu}{\beta}\right)\exp\left(-\exp\left(-\frac{x-\mu}{\beta}\right)\right) \tag{14}$$

with mode $\mu = E\left[\sqrt{J_{2,a}}\right] - 0.5772\,\beta$ and dispersion parameter $\beta = \frac{\sqrt{6}}{\pi}\sqrt{Var\left[\sqrt{J_{2,a}}\right]}$. Then, the probability distribution (14) only depends on the mean $E\left[\sqrt{J_{2,a}}\right]$ and variance $Var\left[\sqrt{J_{2,a}}\right]$ of the amplitude $\sqrt{J_{2,a}}$. Since the variance is $Var\left[\sqrt{J_{2,a}}\right] = E\left[\left(\sqrt{J_{2,a}}\right)^2\right] - E\left[\sqrt{J_{2,a}}\right]^2$, the expression (14) is only a function of $E\left[\sqrt{J_{2,a}}\right]$ and $E\left[\left(\sqrt{J_{2,a}}\right)^2\right]$. In Ref. [71], the mean value $E\left[\sqrt{J_{2,a}}\right]$ is calculated numerically by solving a non-linear equation, which is derived analytically. In this equation, the quantity $E\left[\left(\sqrt{J_{2,a}}\right)^2\right]$ is expressed as function of the expected semi-axes $E[R_i]$ of the smallest hyper-ellipse enclosed to the loading path in the deviatoric space. Even if not mentioned explicitly in [71], the semi-axes $E[R_i]$ are identified by the same definition of EMCE proposed in [67,68] and discussed in Section 3.2 (the only difference is that [71] uses the Daveponrt's formula with bandwidth correction, as suggested in [69]).

The expected semi-axes $E[R_i]$ define the directions of a "principal reference frame" in deviatoric space, which is located by solving an eigenvalue problem; this is actually the same approach proposed in [49,79,80], which represents the theoretical framework of "Projection-by-Projection" spectral method [81] (see next Section 3.3.3).

In Ref. [71], the frequency domain Sines criterion is applied to the finite element analysis of a trail bike suspension arm subjected to a Gaussian random loading (vertical and lateral loading, torque) at wheel connection, which simulate the action of the road irregularity. A linear analysis allows the stress PSD matrix at each note in the finite element model to be calculated from the PSD matrix of the input load. The reliability model based on Sines's criterion is able to provide an overall picture of the most stressed areas in the finite element model, with the associated reliability levels.

3.3.3 "Projection-by-Projection" (PbP) criterion

This multi-axial criterion was first formulated in the time domain [79] and then re-formulated in the frequency domain [80-82]. Without going into the theoretical details, which can be found in other references [81,82], it is useful to recall here only the main idea behind the PbP criterion.

The "Projection-by-Projection" method owes its etymology to the approach used to process a loading path Ψ, which is projected along fixed directions of a "principal reference frame" in the deviatoric space. The directions of the principal frame are found by solving an eigenvalue problem $\mathbf{C}_0 = \mathbf{U}^{\mathrm{T}}\mathbf{C}\,\mathbf{U}$ for the covariance matrix $\mathbf{C}$ of the stress deviator. In the principal frame, the covariance matrix $\mathbf{C}_0$ is diagonal, which means that the stress projections are totally uncorrelated.

The procedure of projecting the loading path then transforms a multi-axial random stress $\mathbf{x}(t)$ into another multi-axial random stress $\boldsymbol{\Psi}(t)$ in deviatoric space, with uncorrelated stress components. Each stress projection is a uniaxial random process and its damage can be estimated by spectral methods for uniaxial processes. As a final step, the damage of each stress projection Ψ_i is summed-up by a non-linear damage rule, to obtain the damage of the multi-axial random stress $\mathbf{x}(t)$.

The method provides a closed form analytical expression to compute the fatigue damage of multi-axial stress, which depends on the uniaxial spectral method used to estimate damage $d(\Psi_i)$ for each projection. For example, by using the TB method, the damage is:

$$d_{\mathrm{TB}}^{\mathrm{PbP}}(\Psi) = \left[\sum_{i=1}^{5}\left(d(\Psi_i)\right)^{2/k_{\mathrm{ref}}}\right]^{\frac{k_{\mathrm{ref}}}{2}} = c_{\mathrm{ref}}^{-1}\Gamma\left(1+\frac{k_{\mathrm{ref}}}{2}\right)\left[\sum_{i=1}^{5}\left(2\lambda_{0,i}\right)\sqrt[k_{\mathrm{ref}}]{\eta_{\mathrm{TB},i}\nu_{0,i}}\right]^{\frac{k_{\mathrm{ref}}}{2}} \tag{15}$$

It is worth noting that the theoretical framework of PbP criterion is very general and it does not impose any choice on the particular spectral method used to compute the damage of each stress projection. Therefore, the damage expression in (15) can easily be rewritten in terms of any other uniaxial spectral methods (e.g. Dirlik expression).

The PbP criterion has been applied to study an L-shaped steel beam under band-limited acceleration [82]. A comparison of results by PbP method and EVMS criterion is shown in Figure 8 and commented in Section 4.1.

4 Special features of multi-axial spectral methods

4.1 Importance of material fatigue properties

A quick survey on experimental data from the literature confirms that almost every material or component has different S/N lines for axial/bending and torsion loading, see Table 2. Two distinct S/N lines must then be defined: one for normal stress and one for shear stress. In Figure 5, σ_A, τ_A are the fatigue strengths at $N_A=2\cdot10^6$ cycles and k_σ, k_τ the inverse slopes.

Please insert here Table 2

Please insert here Figure 5

A multi-axial loading has usually both normal and shear stress components. A uniaxial stress can thus be viewed as the limiting case of a multi-axial loading having just one stress component. For a uniaxial stress, of course, the fatigue life can be estimated directly form S/N data. We can thus expect that, if a uniaxial loading (e.g. bending or torsion) is considered, multi-axial criteria will estimate the same fatigue life as that given by uniaxial S/N data.

This requirement is a sort of "prerequisite" that must be satisfied by (and then considered when formulating) any multi-axial criterion, otherwise inconsistencies or estimation errors may occur. For example, the Matake and Crossland criteria depend on both fatigue limits $\sigma_{\infty\text{-}1}$, $\tau_{\infty\text{-}1}$ for fully-reversed bending and torsion; such criteria are thus consistent with results for uniaxial stress. For infinite life criteria, the fatigue limits provide the necessary information, as the finite-life portion of S/N curves is not of interest. For finite-life criteria, instead, also the inverse slope is information required to fully characterise the finite-life portion of the S/N line, which is necessary to estimate the number of cycles to failure. For example, the PbP method considers a reference S/N line, which is interpolated from S/N lines for bending and torsion. The EVMS criterion, instead, only refers to the S/N line for normal stress. The S/N line for normal stress is also used by the C-S method, which however combines the fatigue limits for bending and torsion to define the PSD of the equivalent stress, see Eq. (11).

It is then interesting to investigate in much more detail whether only a single S/N line (e.g. normal stress) is sufficient, or two S/N lines (e.g. normal and shear stress) are instead necessary to obtain accurate damage estimates.

An answer can be provided by considering, as said before, the limiting case of uniaxial loading. A peculiar example is represented by the Preumont's EVMS discussed in Section 3.1.2. A recent paper [90] tested the accuracy of the Preumont's EVMS criterion against a uniaxial random normal and shear stress, as in bending or torsion loading. For normal stress, the damage d_{eq} estimated by EVMS criterion agrees exactly with the damage d_σ obtained from the S/N line for normal stress. For a uniaxial shear stress, instead, the damage d_{eq} deviates from the damage d_τ calculated with the S/N line for shear stress, the deviation being measured by the ratio:

$$r_d = \frac{d_{eq}}{d_\tau} = \frac{\tau_A^{k_\tau}}{\left(\sigma_A/\sqrt{3}\right)^{k_\sigma}} \frac{\Gamma\left(1+k_\sigma/2\right)}{\Gamma\left(1+k_\tau/2\right)} \left(\sqrt{2V_\tau}\right)^{k_\sigma - k_\tau} \tag{16}$$

which depends on all parameters of S/N lines for normal and shear stress (see Figure 5), as well as on the variance V_τ of the applied random shear stress. In expression (16), the damage d_τ has to be interpreted as the "true" estimation, as it is obtained from the S/N line pertinent to shear stress. A damage ratio r_d=1 means an exact damage estimation by EVMS criterion, regardless of the parameter values in Eq. (16).

A sensitivity analysis has been carried out in Ref. [90] to emphasise the dependence of r_d on the S/N parameters, expressed as ratios k_τ/k_σ and σ_A/τ_A. The results revealed that exact estimations are obtained only at values $k_\sigma=k_\tau$ and $\sigma_A = \sqrt{3}\,\tau_A$ (a condition that in metallic materials is usually an exception, rather than a rule), while very large errors are obtained elsewhere. The numerical results pointed out, in particular, the strong influence of the inverse slopes k_σ, k_τ on the accuracy of damage estimation.

Equation (16) applies also to notched components, provided that the S/N parameters (slope, fatigue strength) are those pertinent to the component S/N line. As it is well known, a notch in a body reduces the fatigue strength and then modifies the S/N parameters of the plain material. The strength reduction is quantified by the fatigue notch factor (or fatigue strength reduction factor) K_f.

For the same notched component, different fatigue notch factors $K_{f,a}$, $K_{f,b}$, $K_{f,t}$ have to be introduced to distinguish between axial, bending and torsion loading. For example, the fatigue strengths of the notched component for bending and torsion are $\sigma_{A,n}=\sigma_A/K_{f,a}$ and $\tau_{A,n}= \tau_A/K_{f,t}$ where σ_A, τ_A are the

fatigue strengths of the plain material (un-notched). Also the inverse slopes of the notched component $k_{\sigma,n}$, $k_{\tau,n}$ are different from those of plain material.

It may then occur that the S/N line of plain material satisfies the condition $k_\sigma=k_\tau$, $\sigma_A=\sqrt{3}\tau_A$, while the S/N line of the notched body does not, i.e. $k_{\sigma,n}\neq k_{\tau,n}$, $\sigma_{A,n}\neq\sqrt{3}\tau_{A,n}$. In this particular case, the accuracy of EVMS criterion would change from plain material to notched component.

Of course, one may argue that the estimation error of EVMS criterion measured by (16) might not actually represent the error for a complex multi-axial loading, as this equation applies only to a uniaxial random shear stress (pure torsion). From one hand, this might be correct, as a pure torsion loading is not a multi-axial loading. On the other hand, we can expect that the estimation error for a multi-axial loading cannot be lower than the error obtained with a pure torsion loading.

Unfortunately, no analytical solution is available to measure the accuracy of EVMS criterion with a multi-axial loading, even for the simple case of biaxial state of stress. Ref. [90] attempted to interpolate the damage ratio for uniaxial random loadings to check the accuracy of EVMS criterion for a combined biaxial normal and shear stress, by introducing the following interpolating function:

$$i_d = r_d + (1 - r_d)\exp\left(-0.5 \cdot v_r\right) \tag{17}$$

where r_d is the damage ratio (16) for pure torsion loading and $v_r=Var(\tau)/Var(\sigma)$ is the variance ratio of shear to normal stress.

Please insert here Figure 6

Figure 6 shows a comparison of the index error i_d over a wide range of v_r values, for different types of materials with plain and notched geometries. A very large error characterises those materials, which have fatigue properties that strongly deviate from the condition $k_\sigma=k_\tau$ and $\sigma_A=\sqrt{3}\tau_A$. An interesting case is represented by welded structural details, where the S/N lines (for the nominal stress approach) have slope $k_\sigma=3$ for normal stress (e.g. bending or tension/compression) and $k_\tau=5$ for shear stress (e.g. torsion loading), as reported in several design codes (e.g. IIW recommendations [91], BS 7608 [92], Eurocode 3 [93]). An example is the welded detail in Figure 7, which has recently been investigated in [88,89]. According to IIW [91], this joint has a FAT category $\Delta\sigma$= 45 MPa for bending (with slope 3) and $\Delta\tau$=80 for torsion (with slope 5). For this joint, the EVMS would give an estimation error r_d=373 for pure torsion loading, see Figure 6.

Please insert here Figure 7

The accuracy of damage estimations with complex multi-axial loading were investigated in [82], which analysed the location of the most damage point in an L-shaped beam as a function of material fatigue properties and local multi-axial state of stress. The damage maps shown in Figure 8 were calculated by the PbP method and the EVMS criterion, by assuming that the L-shaped beam is made of two materials (Material 1, Material 2) having different combinations of S/N curves for bending and torsion loading. The numerical results confirmed that the EVMS is unable to shift the expected location of the most damaged point, when the fatigue properties are changed from one material to another, as shown in Figure 8. This further confirmed the possible inaccuracy of EVMS criterion. Other approaches, as the PbP method, are capable instead to account of any combination of bending and torsion fatigue properties.

Please insert here Figure 8

The errors of Preumont's criterion pointed out in Eq. (16) can be explained by considering that only the S/N line for normal stress is used in fatigue damage computation for the equivalent stress $\sigma_{eq}(t)$, while the torsion fatigue properties are not considered. A simple way to overcome this limitation and to include any combination of material fatigue properties could be the use of a "reference S/N line" calibrated on the S/N lines for both normal and shear stress in a so-called Modified Wöhler Diagram (MWD), see Figure 5, invented by Susmel and Lazzarin [5,94]. As an example, the PbP criterion adopts this formalism and it is shown to provide more consistent results [82]. Another example recently proposed is the criterion using the equivalent Lemaitre stress [95].

4.2 Rotation of principal direction of stress

Multi-axial fatigue analysis has recognised the importance of principal directions of stress. The analysis of a multi-axial loading is further complicated when the principal axes of stress at a point rotate. A very simple example is represented by a cylindrical component subjected to combined bending M_B and torsion M_T. Conventional calculations give the normal and shear stress at any point on the cross section. The orientation of principal stresses will depend, at any time instant, on the

ratio of normal stress to shear stress, which in turn depends on the ratio M_T/M_B at that instant. If both bending and torsion follow in-phase sinusoidal cycles with same frequency, this ratio will not vary and principal directions are then fixed (the loading is called proportional). Instead, introducing a phase shift φ between bending and torsion causes the ratio M_T/M_B to vary with time, thus giving rotating principal axes (the loading is called non-proportional). In constant amplitude loading, the phase shift φ between two harmonic (sinusoidal) loadings at same frequency gives a simple measure of the degree of non-proportionality: a phase angle $\varphi=0$ defines "in-phase" (proportional) loading, a phase angle $\varphi\neq0$ (typically $\varphi=90°$) defines "out-of-phase" (non-proportional) loading.

The loading path of proportional loading is a straight line, while for non-proportional loading it is a circle or ellipse, depending on the relative magnitude of the amplitude of normal and shear stress, respectively. In both cases, the stresses are periodic and the loading path is a closed curve.

This simple definition, however, cannot be applied to random loading. In fact, random loading can be viewed as a superposition of many harmonics, each having a different frequency and phase shift (which are usually spread over a wide interval). Looking at the multitude of phase angles, a random stress would always appear as non-proportional.

In addition, the loading path of random loading is very different to that observed in deterministic (sinusoidal) signals. For example, Figure 9 shows that even highly correlated random loadings (which have, in average, peaks and valleys at same time instants) give a loading path which is all but a perfect straight line; some small deviation (scatter) is present. Not correlated random loading (where peaks and valleys, in average, are shifted) give a loading path which is not a circle, instead it is a coiled and highly irregular curve.

Please insert here Figure 9

The simple example in Figure 9 confirms the need for a statistical approach to describe the phase shift in random loading and to discriminate between proportional and non-proportional loadings. In random loading, phase angles are not suitable to quantify the degree of proportionality and they have to be replaced by their statistical counterpart (i.e. the correlation coefficient).

The correlation coefficient for $x_h(t)$, $x_k(t)$ is defined as $r_{hk} = C_{hk} / \sqrt{V_h V_k}$, where $C_{hk} = Cov\left(x_h(t), x_k(t)\right)$ is the covariance between $x_h(t)$ and $x_k(t)$ (which is equal to the area of the "co-spectrum"), and $V_h=Var(x_h(t))$, $V_k=Var(x_k(t))$ are the variances. Proportional loading have

highly correlated stress components and thus r_{hk}=+1 (the principal axes of stress are fixed in "average"), while non-proportional loading have not correlated stress components and thus have $r_{hk}\neq 1$ (principal axes rotate over time), with typical values r_{hk}=0 and r_{hk}=-1.

The variances V_h, V_k are the areas of the auto-PSDs $S_h(\omega)$, $S_k(\omega)$, which characterise the two random stresses $x_h(t)$, $x_k(t)$ in the frequency domain. The information on the correlation between the two random stresses, instead, is provided by the covariance $C_{hk}=Cov(x_h(t), x_k(t))$, which is the area of the cross-PSD $S_{hk}(\omega)$. Note that $S_{hk}(\omega)$ in general is a complex function of ω; its real part is the "co-spectrum" (which is symmetric in ω), while its imaginary part is the "quad-spectrum" (which is an odd function of ω).

While in constant amplitude loading the angle θ defining the orientation of principal axes is a periodic function of time, in random loading θ takes random values at each time instant, i.e. $\theta(t)$ is a random process.

This explains why, even in proportional loading (r_{hk}=+1), the principal axes are never exactly fixed (the angle θ is not constant over time); they are fixed only in "average", with only small changes around a mean value (see the loading path in Figure 9). In non-proportional loadings (r_{hk}=0) the values of angle θ are spread over a wider interval. The statistical properties of process $\theta(t)$ depend on the statistical properties of the multi-axial random loading.

The degree of non-proportionality of a multi-axial loading can vary from point to point in a mechanical component. This creates a demand for methods that allow a rapid scan of FE models, to measure the orientation of principal stress directions. Spectral methods seem to be very promising. For example, Ref. [66] developed a spectral approach to compute the probability distribution of the angle θ between the principal direction and the x-axis of a local reference frame (the third principal direction z is orthogonal to the xy-plane). Rearranging the equations (44), (47) in [66] into a single expression, the probability distribution θ for a biaxial state of stress can be written as:

$$p_\theta(\theta)=\frac{(1+\tan^2(2\theta))\sqrt{(V_{xx}+V_{yy}-2C_{xx,yy})V_{xy}-\left(C_{xx,xy}-C_{yy,xy}\right)^2}}{\pi\left(\frac{V_{xx}+V_{yy}-2C_{xx,yy}}{4}\tan^2(2\theta)-(C_{xx,xy}-C_{yy,xy})\tan(2\theta)+V_{xy}\right)} \tag{18}$$

where V_{xx}, V_{yy}, V_{xy} are the variances and $C_{xx,yy}$, $C_{xx,xy}$, $C_{yy,xy}$ the covariances of the multi-axial random stress. The function $p_\theta(\theta)$ is clearly periodic of $\pi/2$, which confirms that principal stress directions are mutually orthogonal.

It is interesting to study the behaviour of $p_\theta(\theta)$ for some simple states of stress and especially for the limiting case of uniaxial stress. Figure 10 shows the trends of $p_\theta(\theta)$ when using the statistical parameters in Table 3.

Please insert here Table 3

Please insert here Figure 10

For a normal stress $\sigma_{xx}(t)$ the function $p_\theta(\theta)$ is peaked around θ=0, while for a pure shear stress $\tau_{xy}(t)$ it is peaked around θ=45°, results that are consistent with principal directions found by Mohr's circles. For highly correlated ($r_{xx,xy}$=0.9) normal $\sigma_{xx}(t)$ and shear stress $\tau_{xy}(t)$ the peak moves around 32.5°.

In the simple loading cases in Table 3 the variance of normal and shear stress are close to, but not exactly zero. In fact, it has to be remarked that the function $p_\theta(\theta)$ does not cover the limiting cases of uniaxial stress (e.g. only normal stress $\sigma_{xx}(t)$ or $\sigma_{yy}(t)$, only shear stress $\tau_{xy}(t)$). In fact, for such limiting cases the function goes to infinite. This can be explained by considering that, for these uniaxial stress states, the angle $\theta(t)$ is no longer a random process. For example, when only the stress $\sigma_{xx}(t)$ is present, the principal direction is known to be the x-axis, irrespective of the variance V_{xx} of $\sigma_{xx}(t)$. This result follows from Mohr's circles. Therefore, for this uniaxial normal stress the principal direction is constant at any time instant $\theta(t)$=0 (i.e. it is a deterministic quantity).

In [66], the expression (18) was applied to scan principal stress orientation in an L-shaped beam under random vertical acceleration, see Figure 11. The analysis showed that principal stress directions can vary considerably within the same component. For example, the principal directions in element no. 381 tend to be fixed (the distribution is peaked near θ=0), while in element no. 105 they rotate.

Please insert here Figure 11

The information on the evolution of principal stress directions can also be very useful to discriminate among multi-axial criteria. For example, the literature seems to suggest that critical

plane criteria are most suitable when principal stress directions are fixed, as the physical plane subjected to the maximum shear stress remains fixed in space during loading. On the contrary, criteria based on stress invariants can also be applied when principal stress directions rotate.

On the other hand, a common believe is that the rotation of principal directions causes a change in the rate of damage accumulation, with a strong influence on crack patters and on the fatigue strength of engineering materials. It seems, however, that no general rule can be established, as documented in the literature for constant amplitude loading. For example, it has been observed that out-of-phase loadings do not always determine a decrease of the fatigue strength, as it is commonly presumed (see [5]). A complex interaction occurs among the cyclic change of principal stress directions, cyclic plasticity at microscopic level and the material ductility, which makes difficult to draw general conclusions.

Similar conclusions seem to apply also to random loading; for instance, some experimental data show either a decrease or even an increase in fatigue life for different degrees of correlation among stress components [96-98]. These remarks make one more time clear that "only by running appropriate experiments can the actual material response to non-proportional loading be correctly evaluated" [5].

4.3 Analogies between multi-axial and uniaxial spectral methods

In recent years, some analogies between spectral methods for uniaxial and multi-axial random loading have been investigated. Two recent papers [99,100] suggested the use of multi-axial spectral methods as new tools for estimating the fatigue damage of uniaxial wide-band random stress. The approach proposed in [99,100] requires that the PSD $S(\omega)$ of a uniaxial wide-band stress $x(t)$ is first divided into an infinite set of narrow-band PSDs $S_i(\omega)$, $i=1,...,\infty$, each one centered around the central frequency ω_i, see Figure 12. A uniaxial narrow-band random stress $x_i(t)$ is associated to each $S_i(\omega)$; all processes $x_i(t)$ are mutually not-correlated, as their PSDs $S_i(\omega)$ are jointly not overlapped.

Please insert here Figure 12

The damage of each $x_i(t)$, which is estimated by the “narrow- band formula” [27], is then properly combined to get an expression that is used to estimate the fatigue damage of $x(t)$. The damage expression actually depends on the combination rule used, then a different combination rule would

lead to a different damage expression [99-101]. For example, by using the non-linear damage sum of PbP method in Eq. (15), Ref. [99,100] obtained the damage expression of the "single moment method" for uniaxial random processes:

$$d_{SM} = \frac{2^{k/2}}{2\pi c}\,\Gamma\left(1+\frac{k}{2}\right)\left(\lambda_{2/k}\right)^{k/2} \tag{19}$$

This expression correlates the fatigue damage to just one spectral moment $\lambda_{2/k}$ (where k, c are the S/N parameters) and it is an "empirical" solution that originally was "postulated" from observed simulation trends [30,31]. Ref. [99,100] were thus able to provide a mathematical proof of the "single moment" spectral method. Apart from this result, however, the most relevant outcome of Ref. [99,100] was to establish a formal analogy between uniaxial and multiaxial spectral criteria, which allows the PSD decomposition, followed by a non-linear damage combination rule, to be used as a new approach for fatigue damage estimation in uniaxial wide-band random loading. This new proposal really opens up a new perspective in the fatigue analysis of uniaxial wide-band random processes, as improved spectral methods may be obtained by suitable calibration of the non-linear combination rule in the underlying multi-axial environment after PSD spectral decomposition.

The PSD decomposition and damage combination can also be viewed as a sort of "equivalence criterion", which transforms a uniaxial random stress to a multi-axial one, i.e. the opposite way used by some multi-axial criteria (see Section 3.1), which transform a multi-axial stress to a uniaxial equivalent stress.

5 Conclusions

The discussion in the previous Sections emphasised how multi-axial spectral methods can offer several advantages compared to time domain approaches in the analysis of multi-axial random loadings. For example, spectral methods permit a strong reduction of computational cost, as they allow fatigue damage and life to be estimated directly from PSD data. The "variance method" could be a useful tool to quickly scan the orientation of the critical plane, especially in large FE models. Other multi-axial spectral methods, instead, allow a fast estimate of the fatigue damage directly from the spectral properties (e.g. PSD matrix) of the multi-axial random time-histories of stress.

Spectral analysis can also be used to formulate a probabilistic approach in multi-axial fatigue criteria for random loadings. Interesting examples are the frequency domain EMCC/EMCE spectral

definitions in Section 3.2, which provide a statistical measure of the shear stress amplitude on the critical plane, not affected by the scatter observed in time domain results. Other noteworthy examples discussed in this paper are the frequency domain re-formulations of some multi-axial criteria, e.g. of Matake (Section 3.2.1), Carpinteri-Spagnoli (Section 3.2.2) and Sines (Section 3.3.2). The frequency domain approach also offers a simple way to formulate spectral solutions for multi-axial criteria based on equivalent uniaxial stress, as discussed in Section 3.1

The frequency domain approach is also particularly useful with FE analysis, where spectral methods can replace time domain multi-axial criteria, which have to be applied to the time-histories in each node of the model. The frequency domain approach also allows using a spectral analysis to compute the stress PSDs in each node of the FE model, instead of performing time-consuming simulations necessary to determine the multi-axial stress time-histories.

The purpose of this article, though, was not to convince designers and engineers that a spectral approach is the best solution for any application, as it might wrongly appear from the previous discussion. The engineering judgment must always be used to discriminate among different situations. A critical analysis and some remarks on potential limitations of spectral fatigue analysis are mentioned here, as it is appropriate in Conclusions to list likely sources of error in the proposed methods.

A hypothesis implicitly assumed in spectral analysis is that random time-histories are stationary or almost stationary, which means that they have stable statistical properties over time (this allows a PSD to be defined). Another hypothesis often introduced is that a stationary random history is also Gaussian, as this greatly simplifies the theoretical analysis and allows closed-form expressions to be derived.

One may question, however, to what extent the time-histories measured on real components are close to a stationary Gaussian random process – in other words: does the model fit reality? For example, no measured multi-axial time-history is strictly stationary; it can be stationary, however, if considered over a relatively short time period (which may be seconds, hours or even days, depending on the application). Overloads (e.g. vehicle travelling on a pot-hole) are examples of local deviation from stationarity. Also the hypothesis of Gaussian process is seldom observed in reality, because signals often are intrinsically non-Gaussian (e.g. waves in shallow water), or because a structural non-linearity can transform a Gaussian input loading into a non-Gaussian output stress.

It seems, however, that no spectral solution has been devised so far for non-stationary multi-axial loading, as the existing attempts are only limited to special classes of uniaxial loadings [102, 103]. Instead, spectral solutions for uniaxial non-Gaussian loadings [63,64,104,105] can be extended to multi-axial spectral methods, for example when the fatigue damage of an equivalent uniaxial process has to be estimated (see Sections 3.1.1 and 3.1.4).

Other sources of error in multi-axial spectral methods arise from the use of Palmgren-Miner hypothesis, which is applied almost universally for damage summation when estimating component life, in spite of its known weaknesses. In multi-axial spectral fatigue, Palmgren-Miner rule is used each time spectral methods are applied to estimate the fatigue damage of a uniaxial stress (as almost all the multi-axial criteria discussed in this paper).

Although non-linear damage rules exist [106], spectral methods for uniaxial random loadings rely on the Palmgren-Miner rule because of its simplicity, which allows closed-form analytical damage expressions to be obtained [27]. An empirical correction of the linear rule (Serensen-Kogayev hypothesis) has been used [96], whereas, to the authors' knowledge, only one example of non-linear damage rule has been proposed so far in the literature [107] (at present, non-linear damage accumulation seems far from being solved by spectral fatigue analysis).

On the other hand, non-linear damage rules require that sequence effect in cycle counting is included in damage accumulation, which is a subject that has to be solved in both time domain and frequency domain approaches. The use of a critical damage value less than one (0.5 or even 0.3, as suggested in IIW recommendations [91]) is a practical solution to compensate the errors in Palmgren-Miner rule.

In summary, the above discussion emphasised that, to apply multi-axial spectral methods, some hypotheses or assumptions have to be taken as just first approximations of what observed in reality. Designers and engineers must verify the validity of the hypotheses behind the spectral methods that they are using, to avoid large errors in estimations.

Last, but not least, the importance of experimental testing with different types of multi-axial random loading, as a benchmark to validate the accuracy of spectral approaches, must always be emphasised. Some results are now available in the literature [19,23,36], although further testing has to be carried out to extend the existing experimental database.

References

1 Marquis G. State-of-the-art and future trends in multiaxial fatigue assessment. Mater Testing 2005;47(5):260-266.

2 Bishop NWM, Sherratt F. Finite element based fatigue calculations. NAFEMS; 2000.

3 You BR, Lee SB. A critical review on multiaxial fatigue assessments of metals. Int J Fatigue 1996;18(4):235-244.

4 Papadopoulos IV, Davoli P, Gorla C, Filippini M, Bernasconi A. A comparative study of multiaxial high-cycle fatigue criteria for metals. Int J Fatigue 1997;19(3):219–235.

5 Susmel L. Multiaxial notch fatigue. Woodhead Publishing Limited, UK; 2009.

6 Chu C-C. Multiaxial fatigue life prediction method in the ground vehicle industry. Int J Fatigue 1997;19(supp. 1):S325–S330.

7 Conle FA, Chu C-C. Fatigue analysis and the local stress–strain approach in complex vehicular structures. Int J Fatigue 1997;19(supp. 1):S317–S323.

8 Kocabicak U, Firat M. A simple approach for multiaxial fatigue damage prediction based on FEM post-processing. Mater Des 2004;25:73–82.

9 Papadopoulos IV. Critical plane approaches in high-cycle fatigue: on the definition of the amplitude and mean value of the shear stress acting on the critical plane. Fatigue Fract Eng Mater Struct 1998;21:269–85.

10 Mrzygłód M, Zieliński AP. Numerial implementation of multiaxial high-cycle fatigue criterion to structural optimization. J Theor Appl Mech 2006;44(3):691-712.

11 Weber B, Keunmeugne B, Clement JC, Robert JL. Improvements of multiaxial fatigue criteria computation for a strong reduction of calculation duration. Comp Mater Sci 1999;15:381–399.

12 Bernasconi A. Efficient algorithms for calculation of shear stress amplitude and amplitude of the second invariant of the stress deviator in fatigue criteria applications. Int J fatigue 2002; 24(6):649–57.

13 Bernasconi A, Papadopoulos IV. Efficiency of algorithms for shear stress amplitude calculation in critical plane class fatigue criteria. Comput Mater Sci 2005;34(4):355–68.

14 Susmel L. A simple and efficient numerical algorithm to determine the orientation of the critical plane in multiaxial fatigue problems. Int J Fatigue 2010;32(11):1875–83.

15 Petrucci G. A critical assessment of methods for the determination of the shear stress amplitude in multiaxial fatigue criteria belonging to critical plane class. Int J Fatigue 2015;74:119–31.

16 Li Z, Ringsberg JW, Storhaug G. Time-domain fatigue assessment of ship side-shell structures. Int J Fatigue 2013;55:276–290.

17 Du J, Li H, Zhang M, Wang S. A novel hybrid frequency-time domain method for the fatigue damage assessment of offshore structures. Ocean Eng 2015;98(1):57-65.

18 Benasciutti D, Sherratt F, Cristofori A. Basic principles of spectral multi-axial fatigue analysis. Procedia Engineering 2015;101:34–42.

19 Niesłony A, Macha E. Spectral Method in Multiaxial Random Fatigue. Springer; 2007.

20 Braccesi C, Cianetti F, Lori G, Pioli D. Random multiaxial fatigue: A comparative analysis among selected frequency and time domain fatigue evaluation methods. Int J Fatigue 2015;74:107–118.

21 Crandall SH, Mark WD. Random vibration in mechanical systems. Academic Press Inc., 1963.

22 Rahman MM, Ariffin AK, Abdullah S. Finite element based vibration fatigue analysis of a new two stroke linear generator engine component. Int J Mech Mater Eng (IJMME) 2007;2(1): 63-74.

23 Mršnik M, Slavič J, Boltežar M. Multiaxial vibration fatigue - A theoretical and experimental comparison. Mech Syst Signal Proc 2016;76–77;409–23.

24 Domínguez J, Zapatero J. Effect of the loading spectrum and history length on fatigue life distribution under random loading. Eng Fract Mech 1992;42(6):925-933.

25 Newland DE. An introduction to random vibrations, spectral & wavelet analysis. Dover Publications (3rd edition), 2005.

26 Rodríguez G, Guedes Soares C, Machado U. Uncertainty of the sea state parameters resulting from the methods of spectral estimation. Ocean Eng 1999;26:991–100.

27 Benasciutti D, Tovo R. Spectral methods for lifetime prediction under wide-band stationary random processes, Int J Fatigue 2005;27(8):867-77.

28 Benasciutti D, Fatigue analysis of random loadings: a frequency domain approach, LAP Lambert Academic Publishing, 2012.

29 Dirlik T. Application of computers in fatigue analysis. Ph.D. Thesis, Dept. of Engineering, University of Warwick, UK, 1985.

30 L.D. Lutes, C.E. Larsen, Improved spectral method for variable amplitude fatigue prediction, J Struct Eng ASCE 116(4) (1990) 1149-1164.

31 C.E. Larsen, L.D. Lutes, Predicting the fatigue life of offshore structures by the single-moment spectral method, Probab Eng Mech 6(2) (1991) 96-108.

32 Benasciutti D, Tovo R. On fatigue damage assessment in bimodal random processes, Int J Fatigue 2007;29(2):232-44.

33 Benasciutti D, Tovo R. Comparison of spectral methods for fatigue analysis in broad-band Gaussian random processes. Probab Eng Mech 2006;21(4):287-299.

34 Mršnik M, Slavič J, Boltežar M. Frequency-domain methods for a vibration-fatigue-life estimation - Application to real data. Int J Fatigue 2013;47:8–17.

35 Gao Z, Moan T. Frequency-domain fatigue analysis of wide-band stationary Gaussian processes using a trimodal spectral formulation. Int J Fatigue 2008;30(10–11):1944–1955.

36 Niesłony A, Růžička M, Papuga J, Hodr A, Balda M, Svoboda J. Fatigue life prediction for broad-band multiaxial loading with various PSD curve shapes. Int J Fatigue 2012;44:74–88.

37 Grzelak J, Łagoda T, Macha E. Spectral analysis of the criteria for multiaxial random fatigue. Mat-wiss u Werkstofftech 1991;22:85–98.

38 Będkowski W, Lachowicz C, Macha E. Predicted fatigue fracture plane according to variance method of shear stress under random triaxial stress state. In: Failure Analysis – Theory and Practice, Proc. 7th European Conference on Fracture (ECF 7), Budapest 1988 (ed. E. Czoboly, EMAS UK), vol. I, 281–283.

39 Będkowski W, Macha E. Fatigue fracture plane under multiaxial random loadings – prediction by variance of equivalent stress based on the maximum shear and normal stress. Mat-wiss u Werkstofftech 1992;23:82–94.

40 Łagoda T, Macha E, Dragon A, Petit J. Influence of correlations between stresses on calculated fatigue life on machine elements, Int J Fatigue 1996;18(8):547–55.

41 Preumont A, Piéfort V. Predicting random high-cycle fatigue life with finite elements. J Vib Acoust-Trans ASME 1994;116(2):245-48.

42 Pitoiset X, Preumont A, Spectral methods for multiaxial random fatigue analysis of metallic structures, Int J Fatigue 22(7) (2000) 541–550.

43 Pitoiset X, Preumont A, Kernilis A. Tools for a multiaxial fatigue analysis of structures submitted to random vibrations. Proceedings of the European Conference on Spacecraft Structures, Materials and Mechanical Testing, Braunschweig, Germany, November 1998, pp. 289-294.

44 Pitoiset X, Méthodes spectrales pour une analyse en fatigue des structures métalliques sous chargements aléatoires multiaxiaux, PhD thesis, Université Libre de Bruxelles, 2001 (in French).

45 Allegri G, Zhang X. On the inverse power laws for accelerated random fatigue testing. Int J Fatigue 2008;30(6):967–977.

46 Braccesi C, Cianetti F, Landi L. Random loads fatigue. The use of spectral methods within multibody simulation. Proc. IDETC/CIE ASME 2005, International Design Engineering Technical Conferences & Computers and Information in Engineering Conference, September 2005, pp. 1-11.

47 Sun JQ, Wang X, Bergman LA. Fatigue analysis of non-linear structures with von Mises stress. J Sound Vibr 2001;245(5):947–952.

48 Tovo R, Benasciutti D, Cristofori A, Susmel L. Studio degli approcci in frequenza nella fatica multiassiale ad ampiezza variabile, AIAS Congress, Ancona, September 2006 (in Italian).

49 Cristofori A. A new perspective in multiaxial fatigue damage estimation. PhD Thesis. University of Ferrara, March 2007.

50 Braccesi C, Cianetti F, Lori G, Pioli D. An equivalent uniaxial stress process for fatigue life estimation of mechanical components under multiaxial stress conditions. Int J Fatigue 2008;30(8):1479–97.

51 Niesłony A, Sonsino CM. Comparison of some selected multiaxial fatigue assessment criteria. LBF Fraunhofer Institute, Darmstadt, Report No. FB-234; 2008.

52 Niesłony A. Comparison of some selected multiaxial fatigue failure criteria dedicated for spectral method, J Theor Appl Mech 2010;48(1):233-254.

53 Benasciutti D. An analytical approach to measure the accuracy of various definitions of the "equivalent von Mises stress" in vibration multiaxial fatigue. Proc. of ICOeV Conference, September 2015.

54 Beste A, Dreβler K, Kötzle H, Krüger W, Maier B, Petersen J. Multiaxial rainflow - A consequent continuation of Professor Tatsuo Endo's work. In: The rainflow method in fatigue (ed. Y. Murakami), Butterworth-Heinemann, 1992.

55 Bannantine JA, Socie DF. Multiaxial Fatigue Life Estimation Techniques. Advances in Fatigue Life Prediction Techniques, ASTM STP1122 (eds. M. Mitchell and R. Landgraf), American Society for Testing and Materials, Philadelphia, 1992: 249-275.

56 Dreβler K, Köttgen VB, Kötzle H. Tools for fatigue evaluation of non-proportional loading. In: Proc. of Fatigue Design '95, Helsinki, Finland, 1995.

57 Wang CH, Brown MW. Life prediction techniques for variable amplitude multiaxial fatigue-part 1: theories. J Eng Mater Technol ASME 1996;118:367-370.

58 Wang CH, Brown MW. Life prediction techniques for variable amplitude multiaxial fatigue-part 2: comparison with experimental results. J Eng Mater Technol ASME 1996;118:371-374.

59 Langlais TE, Vogel JH, Chase TR. Multiaxial cycle counting for plane method. Int J Fatigue 2003;25:641-647.

60 Bel Knani K, Benasciutti D, Signorini A, Tovo R. Fatigue damage assessment of a car body-in-white using a frequency-domain approach, Int J Mater Prod Technol 2007;30(1-3):172-198.

61 Susmel L, Tovo R, Benasciutti D. Sulla stima della vita a fatica di giunti saldati soggetti a carichi multiassiali ad ampiezza variabile. Frattura ed integrità strutturale 2009;9:125-134.

62 Susmel L, Tovo R, Benasciutti D. A novel engineering method based on the critical plane concept to estimate lifetime of weldments subjected to variable amplitude multiaxial fatigue loading. Fatigue Fract Eng Mater Struct 2009;32(5):441-59.

63 Benasciutti D, Tovo R. Cycle distribution and fatigue damage assessment in broad-band non-Gaussian random processes. Probab Eng Mech 2005;20(2): 115-127.

64 Benasciutti D, Tovo R. Fatigue life assessment in non-Gaussian random loadings. Int J Fatigue 2006;28(7):733-746.

65 Li B, de Freitas M. A procedure for fast evaluation of high-cycle fatigue under multiaxial random loading. J Mech Des 2002;124:558–63.

66 Pitoiset X, Rychlik I, Preumont A. Spectral methods to estimate local multiaxial fatigue failure for structures undergoing random vibrations. Fatigue Fract Eng Mater Struct 2001;24:715–27.

67 Cristofori A, Benasciutti D. A statistical definition of an equivalent stress amplitude for multiaxial random loadings. Proceedings of the 8th International Conference on Multiaxial Fatigue and Fracture (ICMFF8), Sheffield (UK), 10-14 June 2007.

68 Benasciutti D, Cristofori A. A frequency-domain formulation of MCE method for multi-axial random loadings. Fatigue Fract Eng Mater Struct 22008;31(11):937–48.

69 Preumont A. On the peak factor of stationary Gaussian processes. J Sound Vibr 1985;100(1):15-34.

70 Preumont A. Random vibration and spectral analysis. Kluwer Academic Publishers; 1994.

71 Lambert S, Pagnacco E, Khalij L. A probabilistic model for the fatigue reliability of structures under random loadings with phase shift effects. Int J Fatigue 2010;32:463–74.

72 Bathias C. There is no infinite life in metallic materials. Fatigue Fract Eng Mater Struct 1999;22:559-66.

73 Bathias C, Drouillac L, Le François P. How and why the fatigue S–N curve does not approach a horizontal asymptote. Int J Fatigue 2001;23(1):143–151.

74 Sonsino CM. Course of SN-curves especially in the high-cycle fatigue regime with regard to component design and safety. Int J Fatigue 2007;29(12):2246–2258.

75 Pyttel B, Schwerdt D, Berger C. Very high cycle fatigue – Is there a fatigue limit? Int J Fatigue 2011;33(1); 49–58.

76 Carpinteri An, Spagnoli A. Multiaxial high-cycle fatigue criterion for hard metals. Int J Fatigue 2001;23:135–45.

77 Carpinteri An, Spagnoli A, Vantadori S, Bagni C. Structural integrity assessment of metallic components under multiaxial fatigue: the C-S criterion and its evolution. Fatigue Fract Eng Mater Struct 2013;36(9):870–83.

78 Carpinteri An, Spagnoli A, Vantadori S. Reformulation in the frequency domain of a critical plane – based multiaxial fatigue criterion. Int J Fatigue 2014;67:55–61.

79 Cristofori A, Susmel L, Tovo R, A stress invariant based criterion to estimate fatigue damage under multiaxial loading. Int J Fatigue 2008;30(9):1646–58.

80 Benasciutti D, Cristofori A, L. Susmel, Tovo R. A spectral method for multiaxial random loads. Proc. 8° Int. Conference on Multiaxial Fatigue and Fracture (ICMFF8), Sheffield, 10-14 June 2007.

81 Cristofori A, Benasciutti D, Tovo R. A stress invariant based spectral method to estimate fatigue life under multiaxial random loading. Int J Fatigue 2001;33(7):887–99.

82 Cristofori A, Benasciutti D. "Projection-by-Projection" approach: a spectral method for multiaxial random fatigue. SAE Technical Paper 2014–01–0924.

83 Kurek M, Łagoda T. Comparison of the fatigue characteristics for some selected structural materials under bending and torsion. Mater Sci 2011;47(3):334–344.

84 Atzori B, Berto F, Lazzarin P, Quaresimin M. Multiaxial fatigue behaviour of a severely notched carbon steel. Int J Fatigue 2006;28:485-493.

85 Baier F. Zeit- und Dauerfestigkeit bei überlagerter statischer und schwingender Zug-Druck und Torsionbeanspruchung. PhD Thesis, University of Stüttgart, 1970 (in German).

86 Papuga J, Růžička M. Aiming at stress-based critical plane multiaxial method for finite life calculation, Proc. of the Second International Conference on Material and Component Performance under Variable Amplitude Loading, Darmstadt, March 2009, pp. 465-474.

87 Simbürger A. Festigkeitsverhalten zäher Werkstoffe bei einer mehrachsigen, phasenverschobenen Schwingbeanspruchung mit körperfesten und veränderlichen Hauptspannungsrichtungen. LBF Frauhofer Institute, Darmstadt, Report No. FB-121, 1975 (in German).

88 Bertini L, Cera A, Frendo F. Experimental investigation of the fatigue resistance of pipe-to-plate welded connections under bending, torsion and mixed more loading. Int J Fatigue 2014;68:178–85.

89 Frendo F, Bertini L. Fatigue resistance of pipe-to-plate welded joint under in-phase and out-of-phase combined bending and torsion. Int J Fatigue 2015;79:46–53.

90 Benasciutti D. Some analytical expressions to measure the accuracy of the "equivalent von Mises stress" in vibration multiaxial fatigue. J Sound Vibr 2014;333(18):4326–40.

91 Hobbacher A. et al.. Recommendations for fatigue design of welded joints and components (update). IIW document IIW-1823-07 (ex XIII-2151r4-07/XV-1254r4-07), Paris, October 2008.

92 British Standard BS7608:1993. Code of practice for fatigue design and assessment of steel structures.

93 EN 1993-1-9:2003: Eurocode 3: Design of Steel Structures. Part 1-9: Fatigue.

94 Susmel L, Lazzarin P. A bi-parametric Wöhler curve for high cycle multiaxial fatigue assessment. Fatigue Fract Eng Mater Struct 2002; 25, 63–78.

95 Jingran Ge, Yi Sun, Song Zhou. Fatigue life estimation under multiaxial random loading by means of the equivalent Lemaitre stress and multiaxial S–N curve methods. Int J Fatigue 2015;79:65–74.

96 T. Łagoda, E. Macha, A. Niesłony, Fatigue life calculation by means of the cycle counting and spectral methods multiaxial random loading, Fatigue Fract Eng Mater Struct 2005;28:409–20.

97 Z. Marciniak, D. Rozumek, E. Macha, Fatigue lives of 18G2A and 10HNAP steels under variable amplitude and random non-proportional bending with torsion loading, Int J Fatigue 2008;30(5):800–13.

98 T. Łagoda, E. Macha, Fatigue life under biaxial stress state with different cross-correlation coefficients of normal stress, Proc. of the Ninth Conference on Fracture (ICF 9), Sydney 1997 (eds B.L. Karihaloo, Y.-W. Mai, M.I. Ripley and R.O. Ritchie), vol 3, pp.1371-1378.

99 Cristofori A, Benasciutti D, Tovo R. Analogie fra metodi spettrali e criteri multiassiali nella valutazione del danno a fatica. Proc. of 40° Conference of the Italian Association of Stress Analysis (AIAS), Palermo, Italy, 2011 (in Italian).

100 Benasciutti D, Cristofori A, Tovo R. Analogies between spectral methods and multiaxial criteria in fatigue damage evaluation. Probab Eng Mech 2013;31:39–45.

101 Braccesi C, Cianetti F, Tomassini L. Random fatigue. A new frequency domain criterion for the damage evaluation of mechanical components. Int J Fatigue 2015;70:417-27.

102 Benasciutti D, Tovo R. Frequency-based fatigue analysis of non-stationary switching random loads. Fatigue Fract Eng Mater Struct 2007;30(11):1016-29.

103 Benasciutti D, Tovo R. On fatigue cycle distribution in non-stationary switching loadings with Markov chain structure. Probab Eng Mech 2010;25(4):406-18.

104 Wolfsteiner P, Breuer W. Fatigue assessment of vibrating rail vehicle bogie components under non-Gaussian random excitations using power spectral densities. J Sound Vibr 2013;332(22):5867–82.

105 Rognon H, Bennebach M, Da Silva T, Lefebvre F. Comparison of spectral methods for fatigue analysis in non-Gaussian random processes – Application to elastic-plastic behaviour. Procedia Engineering 2015;101:430–439.

106 Fatemi A, Yang L. Cumulative fatigue damage and life prediction theories: A survey of the state of the art for homogeneous materials. Int J Fatigue 1998;20(1): 9-34.

107 Košút J. Quadratic damage rule in random loading case. Fatigue Fract Eng Mater Struct 2004;27(8):679-700.

FIGURE CAPTIONS

Figure 1. Comparison of experimental results with theoretical estimations obtained by the equivalent strain related to the Smith-Watson-Topper (SWT) and two spectral methods: (a) Dirlik; (b) Tovo-Benasciutti (TB). (Reprinted from Niesłony A et al. Int J Fatigue 2012;44:74–88, with permission from Elsevier).

Figure 2. Symbols used to identify the physical plane Δ in the critical plane criterion developed in Ref. [60].

Figure 3. Minimum Circumscribed Circle (MCC) and Minimum Circumscribed Ellipse (MCE) definitions for: (a) periodic loading path; (b) random loading path. The Expected Minimum Circumscribed Circle (EMCC) and Minimum Circumscribed Ellipse (MCE) definitions are also shown for the random loading path.

Figure 4. Comparison of Minimum Circumscribed Circle/Ellipse (MCC/MCE) with Expected Minimum Circumscribed Circle/Ellipse (EMCC/EMCE) calculated for three replicated random loading paths, having the same correlation between τ_1 and τ_2 stress components : (a)-(c) r_{12}=0.0 (non-proportional); (d)-(f) r_{12}=0.99 (proportional).

Figure 5. A scheme of the Modified Wöhler Diagram, with the S/N lines for normal and shear stress and the reference line for a multi-axial loading.

Figure 6. Damage index i_d in Eq. (17) for different types of plain material and notched specimen.

Figure 7. Tube-flange welded joint studied in Ref. [88,89] (Reprinted from Bertini L et al, Int J Fatigue 2014;68:178–85, with permission from Elsevier).

Figure 8. Damage maps given by PbP method (a)-(b) and EVMS criterion (c)-(d) applied to a L-shaped beam under random acceleration. Comparison of two different materials: (a)-(c) material 1, (b)-(d) material 2.

Figure 9. Example of a biaxial random stress, with different degree of correlation: $r_{\sigma\tau}$=0.99 (proportional loading), $r_{\sigma\tau}$=0.0 (non-proportional loading). The stress variance is $Var(\sigma(t))=3$, $Var(\tau(t))=1$.

Figure 10. Trends of the probability density function $p_\theta(\theta)$ of the angle $\theta(t)$ of principal directions for several states of stress.

Figure 11. Probability distribution $p_\theta(\theta)$ at two different locations in the L-shaped beam under random excitation shown in (a). The local stress is: (b) non-proportional; (c) proportional. (Reprinted from Pitoiset X et al. Fatigue Fract Eng Mater Struct 2001;24:715–27, with permission from Wiley & Sons).

Figure 12. Decomposition of the one-sided PSD $S(\omega)$ into an infinite set of narrow-band infinitesimal spectra $S_1(\omega)$, $S_2(\omega)$, …, $S_i(\omega)$,….

TABLES

Table 1. Results of numerical simulations of multi-axial random stresses: comparison between time domain (deterministic) simulations and frequency domain (statistical) estimations. For each correlation value r_{12}, five replicated loading paths are simulated in time domain.

		Deterministic (time domain)				**Statistical (frequency domain)**			
				MCC	MCE			EMCC	EMCE
r_{12}	**Case**	**R_a**	**R_b**	**$\tau_{a,eq}$**	**$\tau_{a,eq}$**	**E[R_a]**	**E[Rb]**	**E[τ_a]**	**E[τ_a]**
0	1	4.19	4.19	4.19	5.92	4.06	4.06	4.06	5.74
	2	4.36	4.36	4.36	6.16				
	3	4.99	4.47	4.99	6.70				
	4	4.40	4.18	4.40	6.07				
	5	4.27	4.27	4.27	6.05				
0.5	1	4.79	4.79	4.79	6.78	4.97	2.87	4.97	5.74
	2	4.65	4.65	4.65	6.58				
	3	4.73	4.17	4.73	6.31				
	4	4.80	4.80	4.80	6.78				
	5	4.63	4.63	4.63	6.54				
0.99	1	5.36	1.14	5.36	5.48	5.73	0.41	5.73	5.74
	2	6.00	0.43	6.00	6.02				
	3	5.80	0.47	5.80	5.82				
	4	5.52	4.15	5.52	6.90				
	5	5.85	1.12	5.85	5.95				

Table 2. S/N parameters for several plain materials, notched specimens and a tube-flange welded joint.

Type of geometry	Material code	Material type	Ref.	Type of loading [a]	Fatigue strength amplitude at $N_A=2\cdot10^6$ cycles		Inverse slope		σ_A/τ_A	k_τ/k_σ	r_d by Eq. (16)
					σ_A (MPa)	τ_A (MPa)	k_σ	k_τ			
Plain	AlCuMg1	aluminium alloy	[83]	B, T	161	97	7.027	6.868	1.66	0.98	1.109
Plain	C40 (SAE1040)	carbon steel	[84]	A, T	264.2	195.8	17.09	18.2	1.35	1.06	382
Plain	CSN 41 1523 (S355 type)	structural steel	[86]	B, T	231.7	144.5	21.21	15.04	1.60	0.71	0.003
Plain	34CrMo4	medium alloy steel	[85], see [86]	B, T	375	261.1	15.33	11.36	1.44	0.74	0.008
Plain	S20C (AISI 1020 type)	low-alloy steel	[83]	B, T	227	97.8	6.17	6.06	2.32	0.98	0.142
Plain	D-30	aluminium alloy	[83]	B, T	180	120	10.753	9.174	1.5	0.85	0.615
Plain	18G2A (S255 J0)	structural steel	[52]	B, T	189.6	141.9	7.9	12.3	1.34	1.56	$5\cdot10^3$
Plain	CuZn40Pb2	brass	[83]	B, T	216	187	5.857	17.172	1.16	2.93	$2\cdot10^9$
V-notched (r=0.5 mm)	C40 (SAE1040)	carbon steel	[84]	A, T	117.8	152.8	4.62	8.2	0.77	1.77	$5\cdot10^4$
Notched (r=5 mm)	Ck 45 (SAE1045)	carbon steel	[87], see [51]	B, T	357	226	7.7	13.4	1.58	1.74	10^5
tube-flange weld	S355JR steel	structural steel	[88,89]	B, T	45 [b]	80 [b]	3	5	0.56	1.67	374

[a] A=axial, B=bending, T=torsion
[b] stress ranges

Table 3. Statistical parameters of the multi-axial random stress, which are used in the comparison shown in Figure 11. The last two columns show the expected value and standard deviation of process θ(t), calculated from Eq. (18).

Case #	Description	V_{xx}	V_{yy}	V_{xy}	$r_{xx,yy}$	$r_{xx,xy}$	$r_{yy,xy}$	$E[\theta]$ (deg)	std[θ] (deg)
1	pure normal stress σ_{xx}	1	0.001	0.001	0	0	0	1.5	9.98
2	pure shear stress τ_{xy}	0.005	0.005	1	0	0	0	43.3	10.05
3	biaxial normal + shear stress σ_{xx}, τ_{xy}	1	0.001	1	0	0.9	0	30.1	14.39
4	biaxial normal stress σ_{xx}, σ_{yy} + uniaxial shear stress τ_{xy}	1	1	1	0	0	0	24.9	25.87

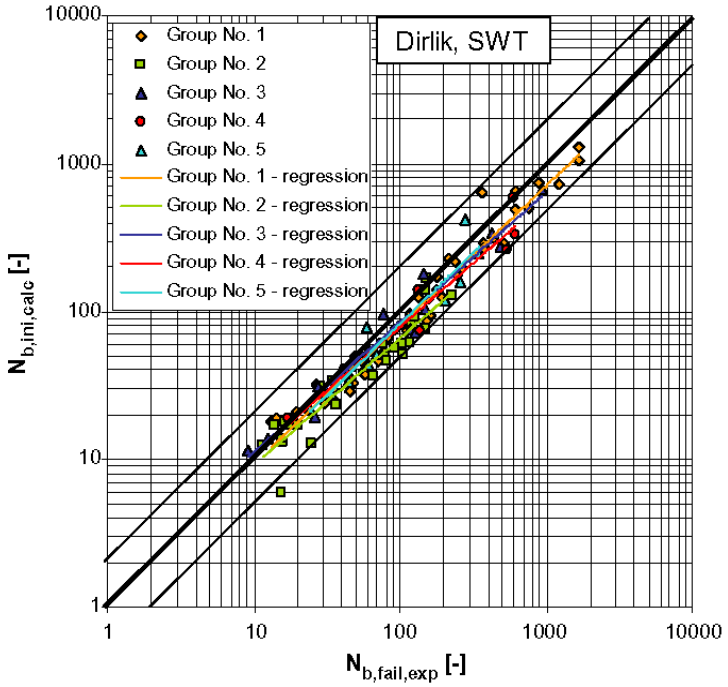
Dirlik, SWT
Group No. 1
Group No. 2
Group No. 3
Group No. 4
Group No. 5
Group No. 1 - regression
Group No. 2 - regression
Group No. 3 - regression
Group No. 4 - regression
Group No. 5 - regression
10000
1000
100
10
1
1
10
100
1000
10000
N b,ini,calc [-]
N b,fail,exp [-]

(a)

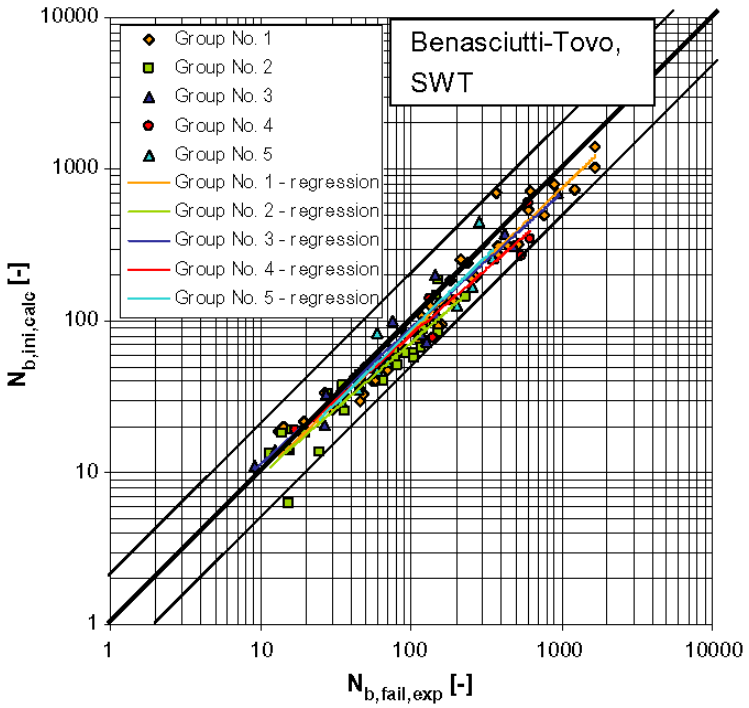
Benasciutti-Tovo, SWT
Group No. 1
Group No. 2
Group No. 3
Group No. 4
Group No. 5
Group No. 1 - regression
Group No. 2 - regression
Group No. 3 - regression
Group No. 4 - regression
Group No. 5 - regression
10000
1000
100
10
1
1
10
100
1000
10000
N b,ini,calc [-]
N b,fail,exp [-]

(b)

Figure 1

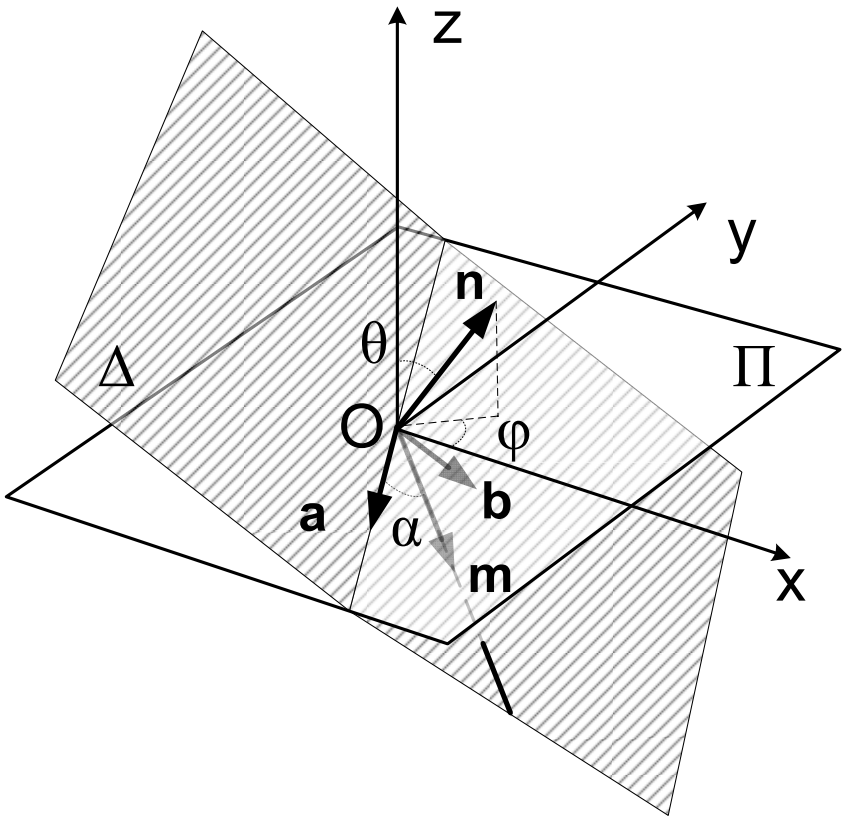

Figure 2

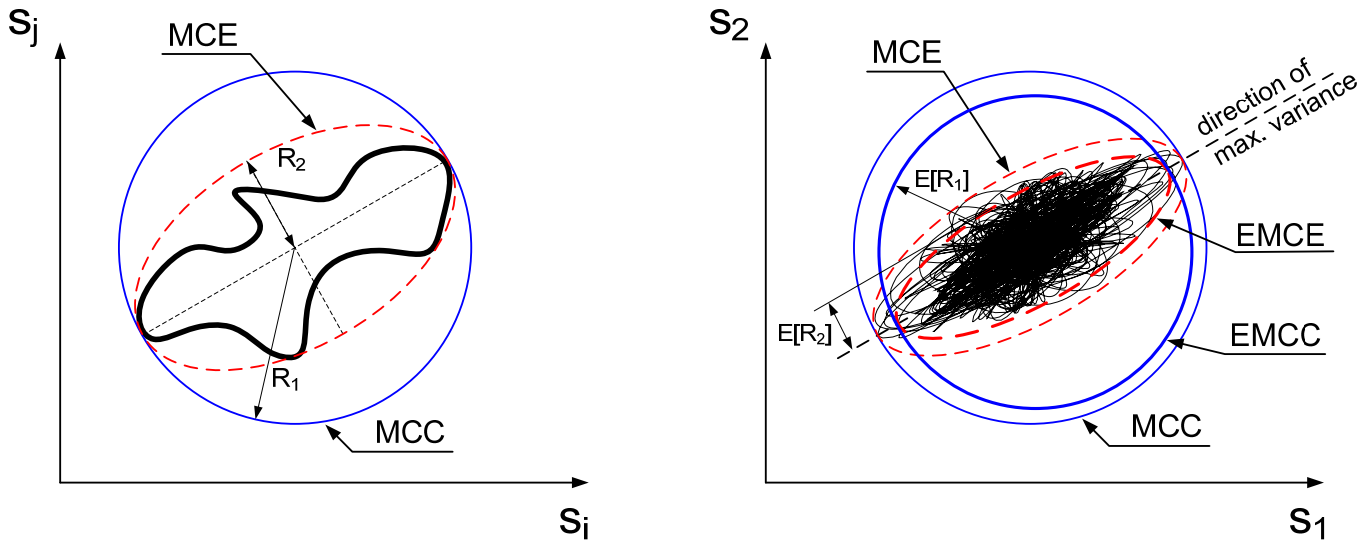
Sj
MCE
R2
R1
MCC
Si
S2
MCE
direction of
max. variance
E[R1]
EMCE
E[R2]
EMCC
MCC
S1

(a) (b)

Figure 3

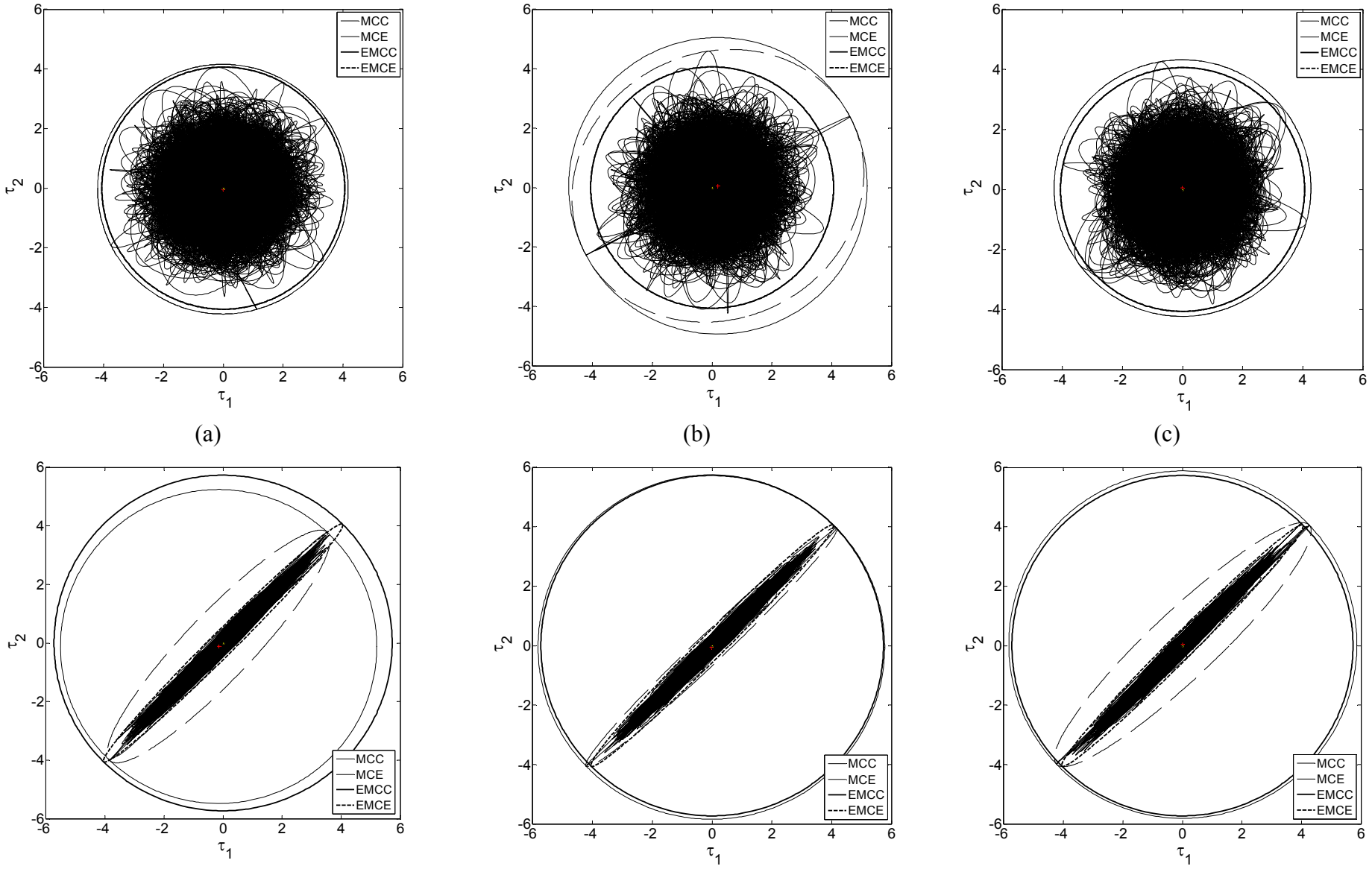

Figure 4

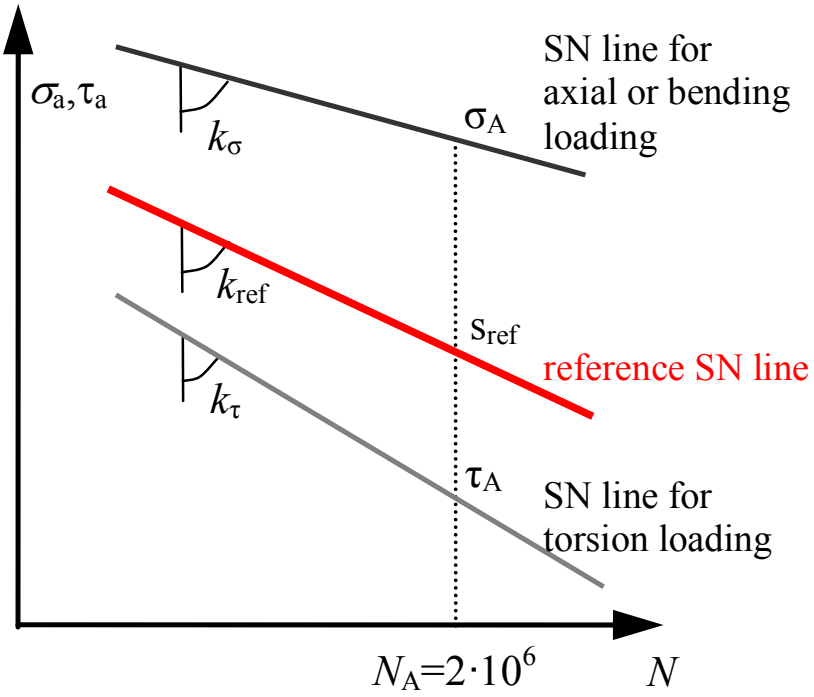
σa,τa
kσ
σA
SN line for
axial or bending
loading
kref
Sref
reference SN line
kτ
τA
SN line for
torsion loading
NA=2·10^6
N

Figure 5

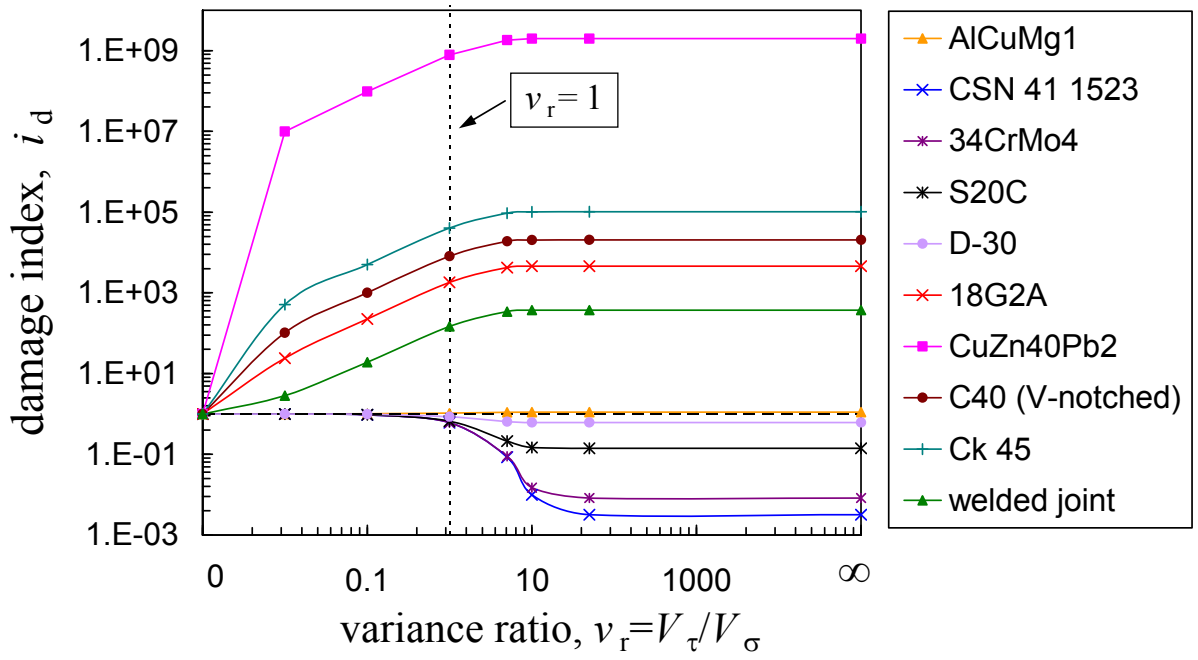
damage index, i_d
1.E+09
1.E+07
1.E+05
1.E+03
1.E+01
1.E-01
1.E-03
$v_r = 1$
0
0.1
10
1000
∞
variance ratio, $v_r = V_\tau / V_\sigma$
AlCuMg1
CSN 41 1523
34CrMo4
S20C
D-30
18G2A
CuZn40Pb2
C40 (V-notched)
Ck 45
welded joint

Figure 6

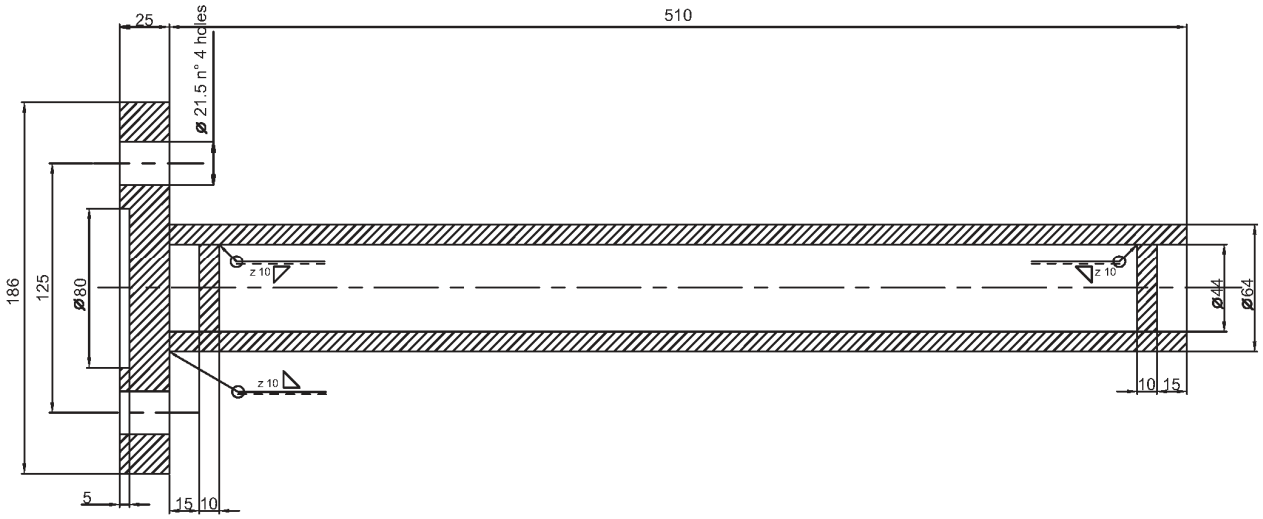

Figure 7

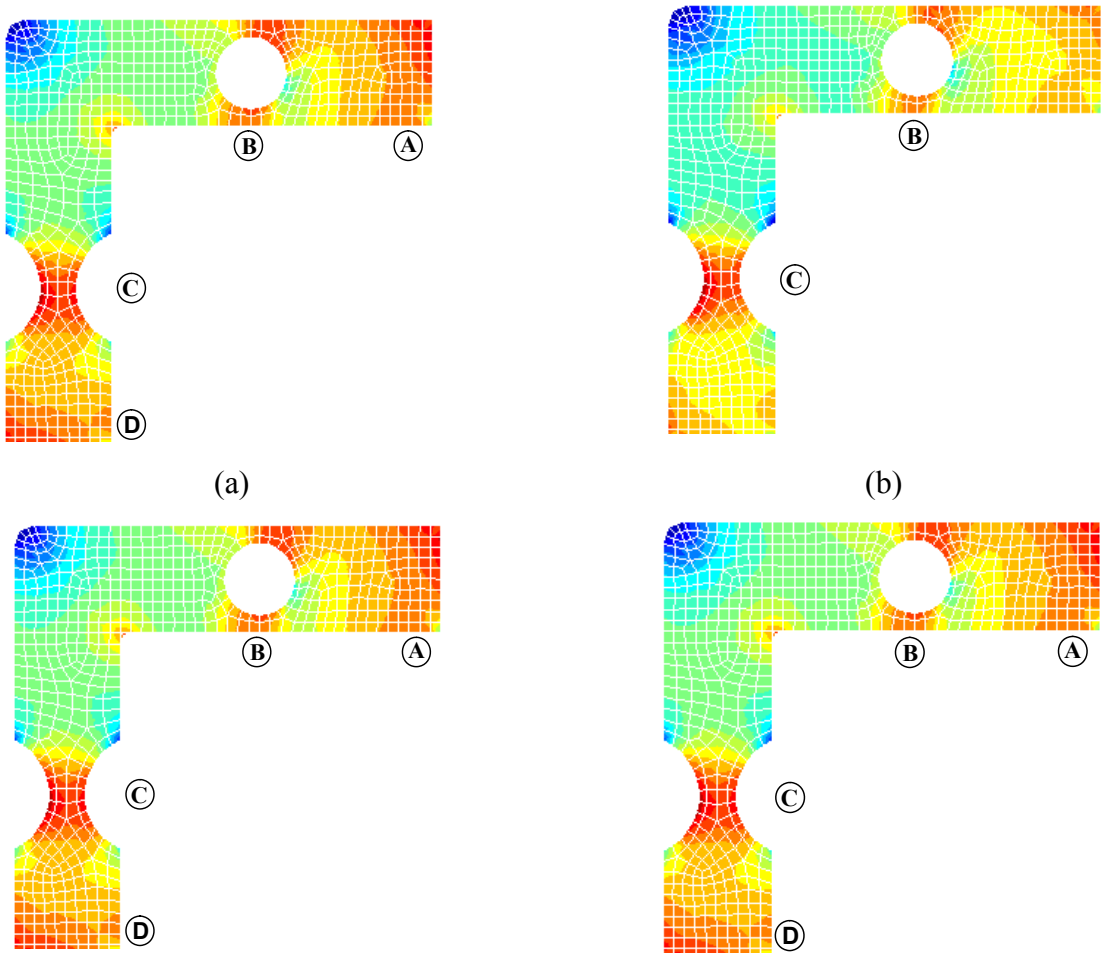

Figure 8

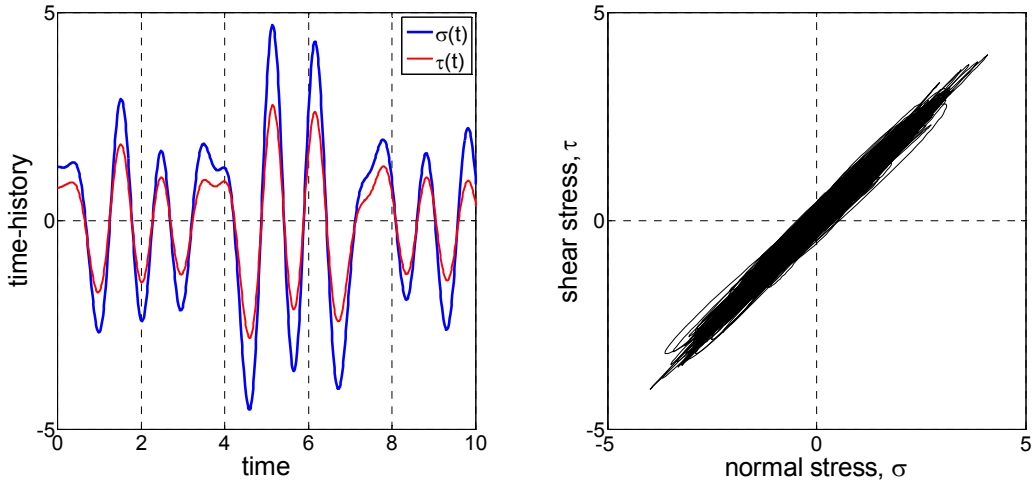
σ(t)
τ(t)
time-history
time
shear stress, τ
normal stress, σ

(a)

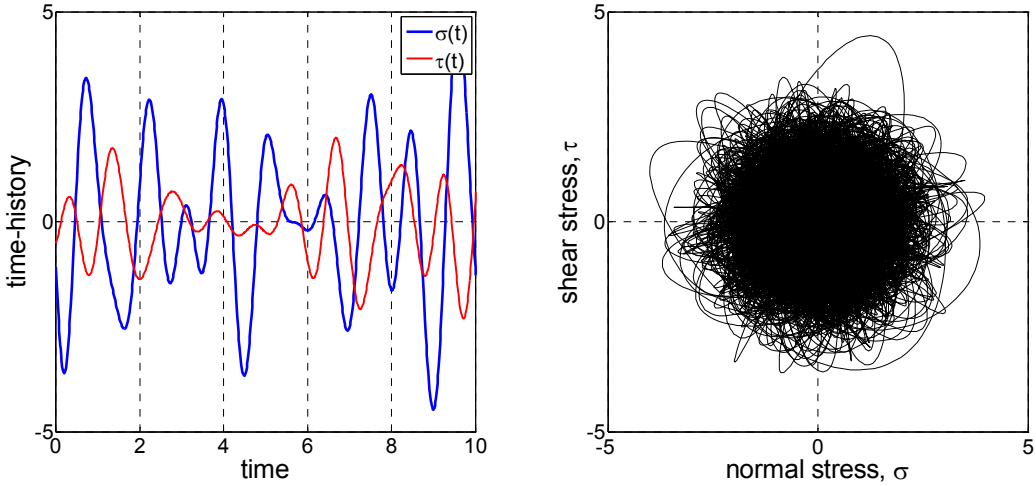
σ(t)
τ(t)
time-history
time
shear stress, τ
normal stress, σ

(b)

Figure 9

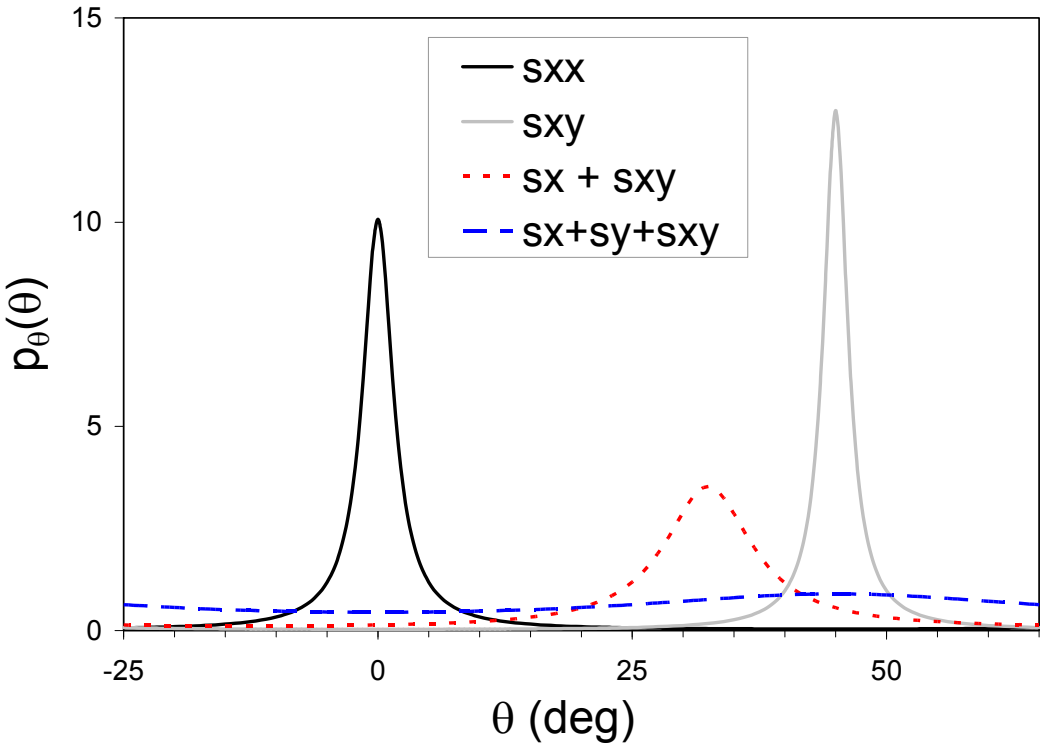

Figure 10

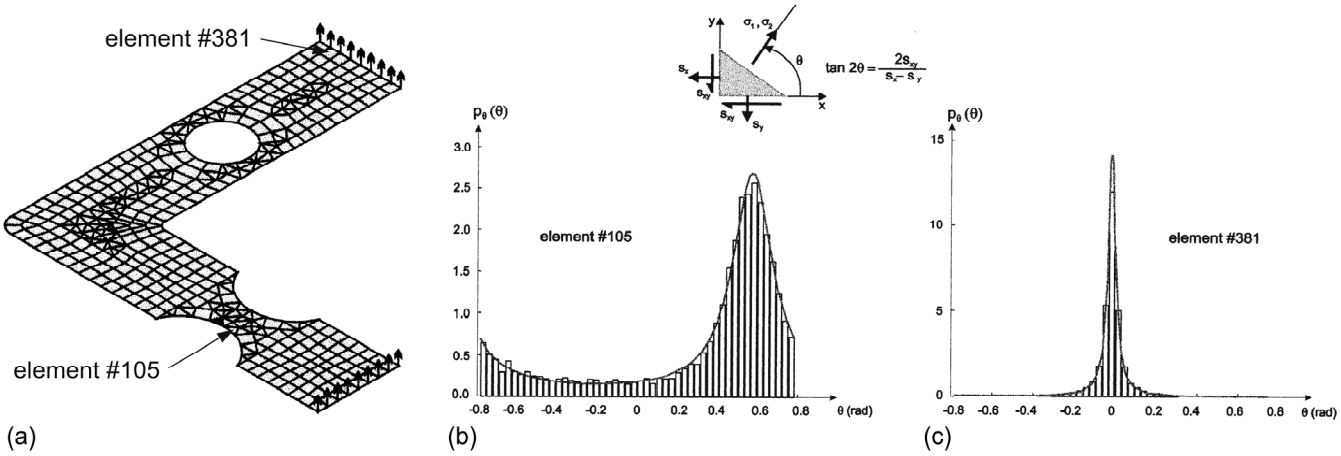
element #381
element #105
(a)
y
σ1, σ2
θ
tan 2θ = 2Sxy / (Sx − Sy)
Sx
Sxy
Sxy
Sy
x
pθ (θ)
element #105
θ (rad)
(b)
pθ (θ)
element #381
θ (rad)
(c)

Figure 11

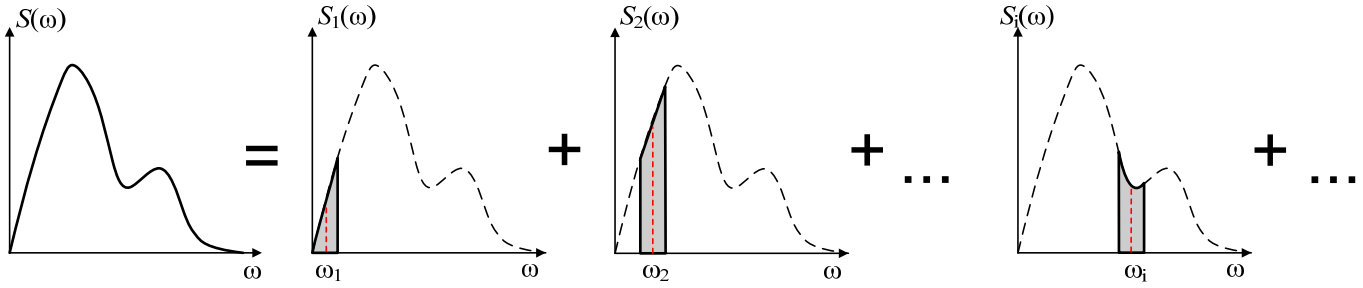

Figure 12